Cellular/Molecular

Upregulated GIRK2 Counteracts Ethanol-Induced Changes in Excitability and Respiration in Human Neurons

Iya Prytkova,[1] Yiyuan Liu,[2] Michael Fernando,[1] Isabel Gameiro-Ros,[1] Dina Popova,[3] Chella Kamarajan,[4] Xiaoling Xuei,[5] David B. Chorlian,[4] Howard J. Edenberg,[5,6] Jay A. Tischfield,[3] Bernice Porjesz,[4] Zhiping P. Pang,[3,7] Ronald P. Hart,[3,8] Alison Goate,[1,2] and Paul A. Slesinger[1]

[1]Nash Family Department of Neuroscience, Icahn School of Medicine at Mount Sinai, New York, New York 10029, [2]Department of Genetics & Genomic Sciences, Icahn School of Medicine at Mount Sinai, New York, New York 10029, [3]Human Genetics Institute, Rutgers University, Piscataway, New Jersey 08854, [4]Department of Psychiatry & Behavioral Sciences, SUNY Downstate Health Sciences University, Brooklyn, New York 11203, Departments of [5]Medical and Molecular Genetics and [6]Biochemistry and Molecular Biology, Indiana University School of Medicine, Indianapolis, Indiana 46202, [7]Department of Neuroscience and Cell Biology and The Child Health Institute of New Jersey, Rutgers Robert Wood Johnson Medical School, New Brunswick, New Jersey 08901, and [8]Department of Cell Biology & Neuroscience, Rutgers University, Piscataway, New Jersey 08854

Genome-wide association studies (GWAS) of electroencephalographic endophenotypes for alcohol use disorder (AUD) has identified noncoding polymorphisms within the *KCNJ6* gene. *KCNJ6* encodes GIRK2, a subunit of a G-protein-coupled inwardly rectifying potassium channel that regulates neuronal excitability. We studied the effect of upregulating *KCNJ6* using an isogenic approach with human glutamatergic neurons derived from induced pluripotent stem cells (male and female donors). Using multielectrode arrays, population calcium imaging, single-cell patch-clamp electrophysiology, and mitochondrial stress tests, we find that elevated GIRK2 acts in concert with 7–21 d of ethanol exposure to inhibit neuronal activity, to counteract ethanol-induced increases in glutamate response, and to promote an increase intrinsic excitability. Furthermore, elevated GIRK2 prevented ethanol-induced changes in basal and activity-dependent mitochondrial respiration. These data support a role for GIRK2 in mitigating the effects of ethanol and a previously unknown connection to mitochondrial function in human glutamatergic neurons.

Key words: alcohol; CRISPRa; excitability; glutamate; *KCNJ6*; mitochondria

Significance Statement

Alcohol use disorder (AUD) is a major health problem, affecting over 100 million people worldwide. While it is known that heritability contributes to AUD, specific genes and their role in neuronal function remain poorly understood. Here, we focused on the inwardly rectifying potassium channel GIRK2, which has been identified in an AUD-endophenotype GWAS. We used human excitatory neurons derived from healthy donors to study the impact of GIRK2 upregulaton. Our results reveal that elevated GIRK2 counteracts ethanol-induced increases in glutamate response and intracellular calcium, as well as deficits in activity-dependent mitochondrial respiration. This role of GIRK2 in mitigating ethanol-induced changes in glutamatergic neuronal offers therapeutic promise for treating AUD.

Received May 10, 2023; revised Jan. 5, 2024; accepted Jan. 11, 2024.

Author contributions: I.P., I.G.-R., D.P., Z.P.P., R.P.H., A.G., and P.A.S. designed research; I.P. performed research; M.F. and R.P.H. contributed unpublished reagents/analytic tools; I.P., Y.L., A.G., and P.A.S. analyzed and discussed data; I.P., Y.L., M.F., A.G., and P.A.S. wrote and edited the paper. D.P., Z.P.P., R.P.H., C.K., X.X., D.B.C, H.J.E., J.A.T., and B.P. commented on the manuscript.

We gratefully acknowledge the support provided by the Ruth L. Kirschstein National Research Service Award (NRSA) Individual Predoctoral Fellowship (1 F31AA027949-01), and Collaborative Studies on the Genetics of Alcoholism (National Institute on Alcohol Abuse and Alcoholism; NIAAA U10AA008401). Special thanks to Dr. Kristen Brennand and Dr. Julia TCW for providing NPC cell lines used in this study. Additional thanks to Dr. Edoardo Marcora for consultation on generalized linear mixed model statistical analysis.

The Collaborative Study on the Genetics of Alcoholism (COGA), Principal Investigators B. Porjesz, V. Hesselbrock, T. Foroud; Scientific Director, A. Agrawal; Translational Director, D. Dick, includes eleven different centers: University of Connecticut (V. Hesselbrock); Indiana University (HJ. Edenberg, T. Foroud, Y. Liu, M. Plawecki); University of Iowa Carver College of Medicine (S. Kuperman, J. Kramer); SUNY Downstate Health Sciences University (B. Porjesz, J. Meyers, C. Kamarajan, A. Pandey); Washington University in St. Louis (L. Bierut, J. Rice, K. Bucholz, A. Agrawal); University of California at San Diego (M. Schuckit); Rutgers University (J. Tischfield, R. Hart, J. Salvatore); The Children's Hospital of Philadelphia, University of Pennsylvania (L. Almasy); Virginia Commonwealth University (D. Dick); Icahn School of Medicine at Mount Sinai (A. Goate, P. Slesinger); and Howard University (D. Scott). Other COGA collaborators include: L. Bauer (University of Connecticut); J. Nurnberger Jr., L. Wetherill, X., Xuei, D. Lai, S. O'Connor, (Indiana University); G. Chan (University of Iowa; University of Connecticut); D.B. Chorlian, J. Zhang, P. Barr, S. Kinreich, G. Pandey (SUNY Downstate); N. Mullins (Icahn School of Medicine at Mount Sinai); A. Anokhin, S. Hartz, E. Johnson, V. McCutcheon, S. Saccone (Washington University); J. Moore, Z. Pang, S. Kuo (Rutgers University); A. Merikangas (The Children's Hospital of Philadelphia and University of Pennsylvania); F. Aliev (Virginia Commonwealth University); H. Chin and A. Parsian are the NIAAA Staff Collaborators. We continue to be inspired by our memories of Henri Begleiter and Theodore Reich, founding PI and Co-PI of COGA, and also owe a debt of gratitude to other past organizers of COGA, including Ting- Kai Li, P. Michael Conneally, Raymond Crowe, and Wendy Reich, for their critical contributions. This national collaborative study is supported by NIH Grant U10AA008401 from the National Institute on Alcohol Abuse and Alcoholism (NIAAA) and the National Institute on Drug Abuse (NIDA).

The authors declare no competing financial interests.

Correspondence should be addressed to Paul A. Slesinger at paul.slesinger@mssm.edu or Alison Goate at alison.goate@mssm.edu.

https://doi.org/10.1523/JNEUROSCI.0918-23.2024

Introduction

A genome-wide association study (GWAS) conducted by the Collaborative Study on the Genetics of Alcoholism (COGA) identified single-nucleotide polymorphisms (SNPs) in the *KCNJ6* gene associated with variations of electroencephalogram (EEG) frontal theta event-related oscillations (θ-EROs) to task-relevant target stimuli during a visual oddball task, in addition to other measures of attention, inhibitory control, and reward processing (Kang et al., 2012; Kamarajan et al., 2017). Low frontal θ-ERO during such tasks is characteristic of individuals with alcohol use disorder (AUD) as well as their high-risk offspring and considered to be an endophenotype for AUD (Jones et al., 2006; Rangaswamy et al., 2007). *KCNJ6* SNPs have also been linked to frontal θ-ERO developmental trajectories during adolescence and young adulthood (Chorlian et al., 2017). These SNPs are noncoding, except for a single imputed synonymous SNP, and therefore are expected to primarily impact gene expression. A recent study investigated a haplotype of 22 linked, noncoding SNPs in the *KCNJ6* gene and found that they are associated with altered expression of *KCNJ6* transcripts and protein in human neurons (Popova et al., 2023).

KCNJ6 encodes a G-protein-coupled inwardly rectifying potassium channel subunit 2, GIRK2 (Kir3.2), which plays a key role in controlling neuronal excitability (Lüscher and Slesinger, 2010). In human brains, GIRK2 is largely present as a homotetramer or in a heterotetramer with GIRK1 (Kir3.1; Lüscher and Slesinger, 2010). The channel is broadly expressed throughout the brain in multiple neuronal types, including cortical pyramidal neurons (Victoria et al., 2016). GIRK2 is coupled to $G_{i/o}$ G-protein coupled receptors (GPCRs), including γ-aminobutyric acid receptor $GABA_B$ and Group II metabotropic glutamate receptors (Lüscher and Slesinger, 2010). Ligand-binding and subsequent dissociation of the G-protein trimer leads to GIRK activation by Gβγ, outward potassium flux, and inhibition of neuronal firing (Lüscher and Slesinger, 2010; Glaaser and Slesinger, 2015). Importantly, alcohol can directly activate GIRK2 via a hydrophobic pocket in the cytoplasmic domain (Aryal et al., 2009; Bodhinathan and Slesinger, 2014; Glaaser and Slesinger, 2015). In addition to these direct mechanisms, GIRK channels depend on phosphatidylinositol 4,5-bisphosphate (PIP_2)-binding and membrane cholesterol to facilitate conformational changes underlying channel activation (Glaaser and Slesinger, 2015, 2017). Studies in mice have shown that GIRK2 affects reward mechanisms and behaviors associated with alcohol and other drugs of abuse (Blednov et al., 2001a,b; Hill et al., 2003; Mayfield et al., 2015).

The direct impact of altered GIRK2 expression on human neurons remains poorly understood. Conceivably, different GIRK2 levels can contribute to changes in neuronal excitability, influencing θ-EROs. To better understand the effect of GIRK2 levels independent of *KCNJ6* SNP haplotypes and AUD genetics, we manipulated the expression of GIRK2 either through CRISPRa (Ho et al., 2017) or with a lentivirus in human glutamatergic neurons derived from healthy donors, facilitating a comparison within the same cell line (i.e., isogenic). We focused on glutamatergic neurons because of the well-documented effects of ethanol on glutamate signaling (Läck et al., 2007; Kim et al., 2010; Das et al., 2016), the frontal cortex associations of GWAS findings (Kang et al., 2012), and SNP expression trait quantitative trait loci effects (https://www.gtexportal.org/home/snp/rs2835872). We hypothesized that elevated GIRK2 expression would influence neuronal adaptations to ethanol exposure.

We used bulk RNAseq to characterize early response to ethanol in glutamatergic neurons with endogenous GIRK2 levels, following a 7 d intermittent ethanol exposure (IEE) protocol (Scarnati et al., 2020). We observed downregulation of genes involved in neuronal development and enrichment of mitochondrial and metabolic pathways. We then tracked the developmental effects of extended (7–21 d) IEE combined with increased GIRK2 expression (↑GIRK2), using multielectrode arrays (MEAs), calcium imaging, patch-clamp electrophysiology, and mitochondrial stress tests to assess glutamatergic function and activity-dependent energy demands. We followed up with bulk RNAseq of 21 d IEE iso-CTL and ↑GIRK2 neurons to identify potential molecular mechanisms underlying the differential adaptations in glutamate sensitivity, membrane excitability, and cellular respiration. Together, our results begin to elucidate the relationship between GIRK2, ethanol, glutamatergic signaling, and mitochondrial health.

Materials and Methods

Resource availability

Lead contact. Further information and requests for resources and reagents should be directed to and will be fulfilled by the lead contact Paul A. Slesinger (paul.slesinger@mssm.edu).

Materials availability. This study did not generate new unique reagents.

Data and code availability. RNAseq data were deposited at NCBI GEO and are publicly available as of date of publication. Accession numbers: GSE226746; GSE244985. Any additional information required to reanalyze data reported in this paper is available from the lead contact upon request.

Experimental model details

Astrocytes. Primary human fetal astrocytes (HFAs) were obtained from a commercial vendor and cultured in astrocyte medium according to the manufacturer specifications (ScienCell, catalog #1801). After cells have reached their terminal duplication capacity, they were transplanted onto 12 mm glass acid-etched coverslips coated in 80 µg/ml Matrigel (Thermo Fisher Scientific, catalog #08-774-552) and cultured for a week to achieve appropriate coverage and attachment.

Neural progenitor cells and induced neurons. Neural progenitor cells (NPCs) and dCas9-VPR NPCs from de-identified control hiPSC cell lines used in this study were derived from both female (cell lines 12455 and 9429) and male (cell lines BJ, 3440, 553-VPR, 2607-VPR) donors (Topol et al., 2016; Ho et al., 2017; Tcw et al., 2017). NPCs and dCas9-NPCs were cultured in DMEM/F12 with sodium pyruvate GlutaMAX medium (Thermo Fisher Scientific, catalog #10565018) supplemented with FGF2 (Bio-Techne, catalog #233-FB), B27 (Life Technologies, catalog #17504-044), N2 (Life Technologies, catalog #17502-048), and penicillin-streptomycin (Thermo Fisher Scientific, catalog #15-140-122). NPCs were induced into neurons with doxycycline-inducible transcription factor *NGN2* with neomycin antibiotic selection (Addgene #99378), following the protocol described by Ho et al. (2016). Antibiotic selection was performed on Day 1 postinduction with 10 µg/ml neomycin sulfate (BioVision Incorporated, catalog #9620). Starting at Day 2 postinduction, induced neurons (iNs) were cultured in Neurobasal medium (Life Technologies, catalog #21103-049) supplemented with N2 and penicillin-streptomycin. At Day 7 postinduction, iNs were infected with *KCNJ6* vector or *KCNJ6* gRNAs in dCas9-VPR expressing cell lines to generate ↑GIRK2 neurons. CRISPRa iso-CTLs were generated using a scramble guide RNA. Lenti cohort controls did not receive any additional viral vector. At Day 10, iNs were dissociated using the Papain Dissociation System following the manufacturer's protocol (Worthington Biochemical, catalog

#LK003153) and then transplanted onto HFA-covered coverslips with thiazovivin (1 µg/ml) (EMD Millipore, catalog #420220) to facilitate attachment. Starting at Day 14, B27 Plus culture system medium (Thermo Fisher Scientific, catalog #A36534-01) supplemented with 2% fetal bovine serum (FBS; Sigma Aldrich, catalog #F3135) and 1% penicillin/streptomycin (Thermo Fisher Scientific, catalog #15-140-122) was introduced through half medium changes every other day to promote electrophysiological maturation.

Method details

KCNJ6 *gRNA design and cloning.* Single gRNAs were designed using CRISPR-ERA (http://crispr-era.stanford.edu/), with the predicted top 6 ranked guides selected for in vitro validation. For lentiviral cloning, IDT synthesized oligonucleotides were annealed and phosphorylated using PNK (NEB#C3019) at 37°C for 30 min, 95°C for 5 min, and ramp-down to 25°C at 5 C/min. Annealed oligos were cloned into lentiGuide-TdTomato-Hygro (Addgene #99376) using BsmB1-v1 (NEB, discontinued) in an all-in-one T7 ligase (NEB#M0318S) based Golden-Gate assembly (37°C for 5 min, 20°C for 5 min ×15 cycles), and subsequently transformed into NEB10beta (NEB#C3019). Purified DNA from propagated colonies were confirmed for gRNA insertion via Sanger sequencing (Genewiz). Following Sanger sequencing confirmation, gRNAs were prepped for lentivirus production.

Lentivirus preparation. Lentiviral vectors were prepared using PEI transfection of HEK-293T cells as previously described (Tiscornia et al., 2006). Viral titer was concentrated to 10^8 IU/ml. Vectors used are listed in Key Resources Table (Addgene #99378, #19780, #99347, #99376, #197032).

Intermittent ethanol exposure. Starting at Day 21 postinduction, 100% ethanol (EtOH; Sigma Aldrich, catalog #e7023) was added to B27 Plus System culture medium to achieve a final concentration of 17 mM. A previous study demonstrated that after 24 h, ethanol concentration in medium is reduced to ∼5 mM, and therefore medium was "spiked" with 1 µl EtOH/1.5 ml medium daily to maintain ∼17 mM concentration, producing an intermittent ethanol exposure (IEE) (Halikere et al., 2020; Scarnati et al., 2020).

Bulk RNAseq. *NGN2*-induced neurons were scraped from 12-well plates at 28 or 42 d of differentiation, spun down, and frozen. Total RNA extraction from frozen cell pellets, library preparation, and sequencing was performed by Genewiz (Azenta US). Total RNA was extracted from fresh frozen cell pellet samples using Qiagen RNeasy Plus Universal mini kit following manufacturer's instructions (Qiagen). RNA samples were quantified using Qubit 2.0 Fluorometer (Life Technologies), and RNA integrity was checked using Agilent TapeStation 4200 (Agilent Technologies). RNA sequencing libraries were prepared using the NEBNext Ultra RNA Library Prep Kit for Illumina using manufacturer's instructions (NEB). The samples were sequenced on the Illumina 4000 instrument, using a 2 × 150 bp Paired End (PE) configuration. Image analysis and base calling were conducted by the Control software. Raw sequence data (.bcl files) generated the sequencer were converted into fastq files and demultiplexed using Illumina's bcl2fastq 2.17 software.

Raw reads were assessed for quality using FastQC (version 0.11.8) before and after adapter sequence trimming by Cutadapt (version 4.1). Reads were pseudoaligned using Salmon (version 0.13.1) for estimation of normalized gene expression (TPM, i.e., transcript per million). Reads were also aligned to the human reference genome (Gencode version 28) and quantified for gene read counts, both in STAR (version 2.5.3a). In Day 28 neurons' differential gene expression analyses, read counts were modeled in the linear mixed model using batch, sex, and donor information as the random effect terms and ethanol treatment/control as the fixed effect term by the R (version 4.1.0) package "variancePartition" (version 1.28.0). In Day 42 neurons, differential gene expression analysis was conducted using the NOISeq package in R (version 2.42.0; Tarazona et al., 2015), correcting for batch and donor effects, with ↑GIRK2 + IEE groupwise comparison to untreated isogenic controls. In Day 28 neurons, gene set enrichment analysis (GSEA) was performed with 1,000 permutations using R package GOtest (github.com/mw201608/Gotest) in the human molecular signatures database "C2.CP", "C5.BP", "C5.CC," and "C5.MF" collections. In Day 42 neurons, synaptic pathway analysis was performed using SynGO online portal (version 1.2; Koopmans et al., 2019).

Western blot. Tissue from 28-day-old neurons was collected by scraping, and membrane protein was extracted using MemPer Thermo Fisher kit (Thermo Fisher Scientific, catalog #89842) according to the manufacturer's instructions. The membrane fraction was then denatured for 20 min at 70°C in MES running buffer (Life Technologies, catalog #B0002) and separated on a BOLT 4–12% Bis-Tris 1 mm gel (Thermo Fisher Scientific, Invitrogen, catalog #NW04125BOX) at 200 mV for 20–30 min. Transfer to a nitrocellulose membrane was achieved using iBlot 2. Membranes were then blocked in 5% milk in PBST for 1 h. To ensure antibody specificity, we utilized antigen competition as a control, where the antibody (Alomone Labs, catalog #APC-006) was preincubated with the antigen in the blocking solution for 1 h on ice; 1:3 antibody to antigen ratio was used. Anti-NaK-ATPase antibody (Cell Signaling Technology, catalog #23565S) was used as a loading control. Membranes were incubated in 1:500 antibody or antibody/antigen mixture overnight at 4°C. Anti-rabbit-HRP secondary antibody (Cell Signaling Technology, catalog #7074P2) at 1:1,000 dilution was incubated for 1 h at room temperature. WesternBright peroxidase (Advansta, catalog #K-12045-D20) 2 min incubation and 90 s exposure on UVP imager were used to obtain images.

Immunocytochemistry. Neurons at Day 28 were fixed in methanol for 20 min at −20°C, followed by permeabilization in 0.2% Triton X-100 in PBS (Mg^{2+}, Ca^{2+}), and blocking in 2% bovine serum albumin, 5% normal goat serum, and 2% Triton X-100 in PBS (Mg^{2+}, Ca^{2+}) at room temperature. Primary antibodies were diluted in 4% NGS, 0.1% Triton X-100 in PBS [no Mg^{2+}, Ca^{2+}; GIRK2 (Alomone Labs, catalog #APC-006) 1:400, TUJ1 (BioLegend, catalog #801213, RRID: AB_2728521) 1:1,000] and incubated overnight at 4°C. Secondary antibodies were incubated for 2 h at room temperature at 1:500 dilution [anti-rabbit Alexa Fluor 488 (Thermo Fisher Scientific, catalog #A-11008, RRID: AB_143165), anti-mouse Alexa Fluor 647 (Thermo Fisher Scientific, catalog #A-21235, RRID: AB_2535804)]. Images were acquired at the Icahn School of Medicine Microscopy and Advanced Bioimaging Core, using the Zeiss Upright LSM-780, Axio Imager 2 confocal microscope with the 100× objective. Maximum intensity projection was obtained from Z-stacks consisting of 5–15 6.6 µm slices, using Zeiss Zen Black software. The maximum intensity projection image was analyzed using Analyze Particles in FIJI (ImageJ; Schindelin et al., 2012).

Multielectrode array. CytoView 48-well MEA plates (Axion Biosystems, M768-tMEA-48B) were coated with 80 µg/ml Matrigel (Thermo Fisher Scientific, catalog #08-774-552) and seeded with HFAs (ScienCell, catalog #1801). Neurons were transplanted on Day 10 of induction. The plate was loaded onto the Axion Maestro MEA reader (Icahn School of Medicine at Mount Sinai Stem Cell Engineering Core), and the electrical activity was analyzed using AxIS 2.0 Neural Module software. Ten minute MEA recordings (Ho et al., 2016; Soni et al., 2021) were acquired on Days 28, 35, and 42 postinduction, at ∼24 h after last ethanol supplementation (Fig. 3*B*), which is estimated to be ∼5 mM after ∼24 h (Scarnati et al., 2020). Wells with little or no activity (<0.01 Hz) were excluded from analysis. One outlier data point was identified by the Grubbs outlier test and removed from further analysis (Fig. 3*D*).

Patch-clamp electrophysiology. Day 42 neurons were recorded at room temperature (∼20°C) in artificial cerebrospinal fluid (ACSF) external solution consisting of the following (in mM): 125 NaCl, 5 KCl, 10 D-glucose, 10 HEPES-Na, 3.1 $CaCl_2$, and 1.3 $MgCl_2{\cdot}6H_2O$. Solution pH was adjusted to 7.4 with NaOH and filtered with 0.22 µM PEI bottle-top filter. Osmolarity was measured at 290–300 mOsm with VAPRO Vapor Pressure Osmometer (Fisher Scientific, ELITechGroup Model 5600, catalog #NC0044806). Patch pipettes were pulled to a resistance of 4–4.5 MΩ. GIRK current was recorded with an internal solution

containing the following (in mM): 140 K-D-gluconate, 4 NaCl, 2 $MgCl_2{\cdot}6H_2O$, 1.1 EGTA, 5 HEPES, 2 Na_2ATP, 5 Na-creatine-PO_4, and 100 GTPyS. pH adjusted to 7.4, and osmolarity was measured at 300–310 mOsm. EPSCs were recorded gap-free at −70 mV using voltage clamp with an internal solution of the following (in mM): 135 $CsCl_2$, 10 HEPES-Na, 1 EGTA, 1 GTP-Na, and 1 QX-314 as described by Yang et al. (2017). All electrophysiology chemicals were purchased from Sigma.

Resting membrane potential was obtained in current-clamp mode ($I = 0$). Cells with a resting membrane potential higher than −40 mV and a membrane resistance lower than 100 MΩ were excluded from further recordings and analyses. For measuring excitability, the membrane potential was adjusted to −55 mV (equivalent to −72 mV with a junction-potential correction of 17 mV). Neuronal excitability was measured with current injection steps of 20 pA (up to 16 steps). Rheobase was defined as the voltage at which the first current injection step elicited an action potential first. Neurons with fewer than two action potential spikes were excluded from further analysis. In voltage clamp, GIRK currents were assessed using a 100 ms voltage ramp (from −100 to 0 mV) to examine inward rectification of GIRK channels, followed by 300 ms pulse at −40 mV to measure the outward GIRK current, and a 20 ms step to −45 mV to monitor membrane resistance, from a holding potential of −40 mV. Voltage pulses were delivered every 2 s at a sampling rate of 5 kHz and low-pass filter frequency of 2 kHz. After 4–5 min 30 µM SCH-23390 (Fisher Scientific, catalog #092550) in ACSF was applied for 1 min, followed by a 2 min ACSF washout. All data were acquired using the Clampex software (v11.0.3.3, Molecular Devices) with an Axopatch B200 amplifier and Digidata 1550B digitizer with HumSilencer enabled to minimize noise. EPSCs were analyzed with Easy Electrophysiology software (v2.5.2, Easy Electrophysiology). GIRK current quantification and I-clamp data were analyzed in Clampfit software (v10.7.0.3, Molecular Devices). The amplitude of GIRK current was measured as an average of 20 ms at −40 mV, ∼150 ms after the voltage ramp.

Seahorse assay. Assays were conducted at the Icahn School of Medicine Mitochondrial Analysis Facility, using an XFe96 Agilent Seahorse Analyzer. NPCs were plated directly in 96-well Agilent Seahorse Cell Culture plates (Agilent Technologies, catalog #101085-004), coated with Matrigel, and induced into neurons the following day. Each cell line was plated in eight-replicate wells for each experiment. On the day of the experiment, neurons were incubated for 1 h in CO_2-free incubator in Agilent Seahorse DMEM assay medium (Agilent Technologies, catalog #103575-100) supplemented with 1 mM sodium pyruvate (Agilent Technologies, catalog #103578-100), 10 mM glucose (Agilent Technologies, catalog #103577-100), and 2 mM glutamine (Agilent Technologies, catalog #103579-100). Acute 10 µM glutamate injection was applied to four-replicate wells/donor/experiment during the mitochondrial stress test (Agilent Technologies, catalog #103015-100). The mitochondrial stress test was performed according to the manufacturer's protocol, with 1 µM oligomycin, 1 µM FCCP, 1 µM rotenone/antimycin-A. Data were acquired in Seahorse Wave software (Agilent Technologies).

After conclusion of the experiment, medium was aspirated and cells were fixed with methylene blue overnight at 4°C. The dye was rinsed out the following morning with distilled water, and cells were lysed with 4% acetic acid and 40% methanol. The lysate was transferred to a clear flat-bottom 96-well plate to measure absorbance at 595 nm using a Varioskan plate reader (Thermo Scientific, catalog #VL0000D0) and SkanIt software for Microplate Readers, ver. 6.0.2.3 (Thermo Scientific, catalog #5187139). Absorbance values were applied as a scaling factor for raw oxygen consumption rate (OCR; pmol/min) to normalize respiratory rate to cell density. Normalized raw data were exported as an Excel spreadsheet for further analysis in R Studio, v3.6.1 (R Core Team, 2020). Mitochondrial respiration parameters were calculated according to the mitochondrial stress test assay user manual. Each experiment replicate is reported as the average of four wells.

Calcium imaging. Neurons were incubated in 4 µM Fluo4-AM in ACSF (same solution as for patch-clamp electrophysiology) for 20 min at 37°C, protected from light. Cells were then destained for an additional 5 min in ACSF at room temperature prior to imaging. Fluorescence was measured with at 10× objective on a Nikon TE2000 inverted microscope, 480 nm (Mic-LED-480A, Prizmatix), an HQ480/40x excitation filter, and a HQ535/50m emission filter. Images were obtained with a sCMOS Zyla 5.5 camera (Oxford Instruments, Andor), using a 10 fps rate and 4 × 4 binning under constant perfusion of ACSF in a laminar flow diamond-shaped chamber (model RC-25; Warner Instruments) at RT (∼20°C). Spontaneous activity was recorded for 3 min. and 10 µM glutamate in ACSF was applied in 30 s pulses, with a 1 min ACSF washout period. A total of 15 mM KCl in ACSF was applied at the end of the recording for 1 min, followed by a 1 min ACSF washout. Time of stimulus application was tagged during the recording.

Raw fluorescence data were collected using Nikon Elements software (NIS-Elements AR; version 5.20.01). A background region of interest (ROI) was identified to subtract noise. ROIs were identified using automatic detection in Nikon Elements. All ROIs were manually curated and raw fluorescence data were exported into Excel. Subsequent analysis steps were carried out in R Studio (v3.6.1 of R). Each fluorescence trace was corrected for baseline drift using a penalized least-squares algorithm with lambda = 10 (AirPLS; Zhang et al., 2010), and $\Delta F/F_0$ was calculated according to the formula $(F_t - F_0)/F_0$, where F_0 was defined as the minimum fluorescence intensity (RFU) in the first 10 s of the recording. Traces were filtered with a 3rd order Butterworth filter using "signal" package version 0.7-6 (Ligges et al., 2021), and spikes were detected using "Pracma" package version 2.3.3 (Borchers, 2022; Extended Data Fig. 4-1). A neuronal spike was defined as <30 s in duration and above 5 standard deviations of the background ROI. ROIs with astrocyte-like spikes (lasting >30 s) were excluded from the analyses. ROIs without any detectable spikes were also excluded.

Experimental design and statistical analyses

Sample size of 4–6 donors and isogenic design was selected to maximize sensitivity and minimize the false discovery rate, as shown by Germain and Testa (2017). The experimenter was not blinded to experimental conditions during data collection and analysis. All statistical analyses were carried out in R Studio, v3.6.1 (R Core Team, 2020), using the following packages for quantitation and visualization: jtools version 2.1.4 (Long, 2022), lme4 version 1.1-27.1 (Bates et al., 2022), and ggplot2 version 3.3.5 (Wickham et al., 2023). One-tailed Student's t test was used for immunocytochemistry puncta % μm^2 quantitation, with a $p = 0.05$ significance cutoff. Generalized linear mixed models (GLMMs) were used for patch-clamp electrophysiology, MEA, calcium imaging, and mitochondrial stress test data to account for donor and batch replicate effects. GLMM analysis maintains appropriate biological grouping of variables (i.e., donors) and can account for random variance between replicate experiments, while still retaining the full power of multiple measurements (e.g., neuronal ROIs in calcium imaging; Popova et al., 2023). Additionally, utilizing GLMM permits the specification of different distributions of data, unlike ANOVA, which relies on the assumption of a normal distribution (Yu et al., 2022). Data normality was tested using the Shapiro–Wilk test. Random effects included donor cell line, neuronal differentiation batch, and/or experimental replicates (e.g., coverslips for calcium imaging and patch-clamp electrophysiology data). Fixed variables included GIRK2 expression level and ethanol exposure, tested for separate and interaction effects, with a $p = 0.05$ significance cutoff. Model fit was selected based on lowest AIC (Akaike information criterion) values. Poisson distribution was specified for all spike count data. Representative formula: Spikes ∼ GIRK2*EtOH + (1|Donor) + (1|Batch), family = "poisson". All bar and line plots include ±standard error of the mean, with individual datapoints shown for each replicate and color-coded by donor.

Results

Enhancing GIRK2 currents in human neurons using CRISPRa and lentivirus expression of *KCNJ6*

To study the effect of increased GIRK2 expression on neurogenin 2 (*NGN2*)-induced glutamatergic neurons (Ho et al., 2016, p. 2) and their response to chronic ethanol exposure, we employed two different methodologies: dCas9-VPR activation (CRISPRa; Ho et al., 2017) of the *KCNJ6* gene and expression from a lentivirus. CRISPRa has the advantage of upregulating the endogenously encoded *KCNJ6* gene, but it relies on stable expression of the dCas9-coupled transcriptional activator VPR and chromatin accessibility of the endogenous gene (Ho et al., 2017; Savell et al., 2018). Lentiviral vector-mediated expression bypasses these limitations but expresses the *KCNJ6* mRNA without the 3′UTR, which may play a key role in protein trafficking to the plasma membrane as well as transcript stability (Loya et al., 2008).

We therefore evaluated the effect of both strategies on GIRK2 expression and function in *NGN2*-induced neurons using qPCR, Western blotting, and immunocytochemistry. The endogenous levels of GIRK2 protein appeared low, with average puncta density of 2.2 ± 0.5% of neuronal marker β-III tubulin (TUJ1)-immunoreactive area (μm^2). CRISPRa was accomplished using cell line 553 stably expressing dCas9-VPR (Ho et al., 2017) and coexpression of three pooled gRNAs targeting the *KCNJ6* promoter (see Materials and Methods; Fig. 1*A*,*B*). In comparison to 553/dCas9-VPR alone, GIRK2 puncta density increased to 23 ± 3% ($p = 0.009$; $N = 9$ iso-CTL, 16 ↑GIRK2) of TUJ1 area in 553/dCas9-VPR + *KCNJ6* gRNAs (CRISPRa). For lentiviral (Lenti) expression of *KCNJ6*, we used a lentivirus containing the *KCNJ6* gene with mCherry red fluorescent marker in cell line 12,455 (control line from Knight Alzheimer's Disease Research Center; Tcw et al., 2017). Here, we observed an increase in GIRK2 puncta density to 24 ± 6% ($p = 0.005$; $N = 9$ iso-CTL, 10

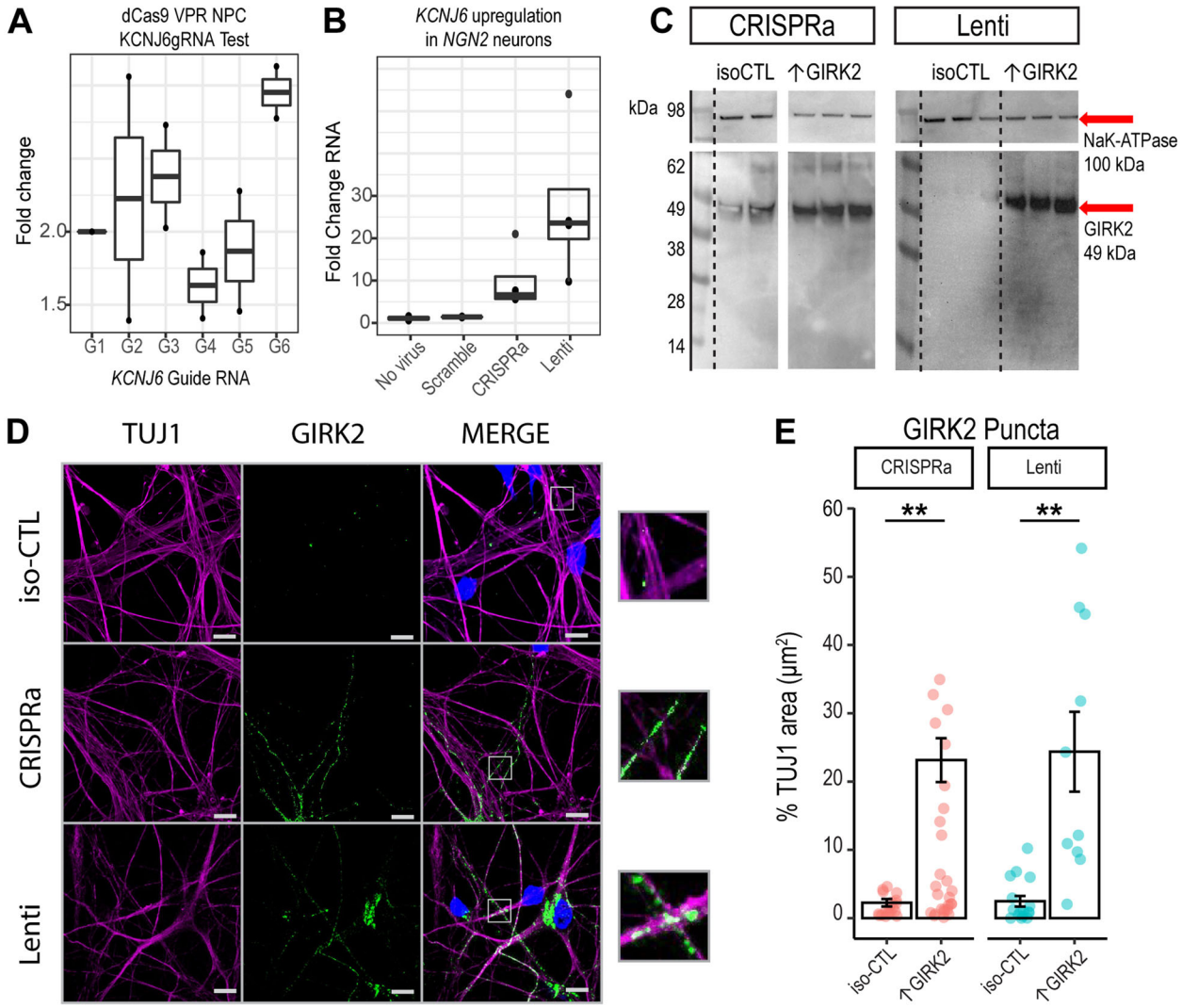

Figure 1. CRISPRa and lentivirus-mediated *KCNJ6* expression similarly increase GIRK2 protein in human glutamatergic neurons. ***A***, RT-qPCR test of 6 *KCNJ6* gRNAs normalized to a scramble gRNA control in D42 *NGN2* neurons ($N = 1$ donor, 2 replicates). ***B***, RT-qPCR of *KCNJ6* expression in D42 *NGN2* neurons with scramble gRNA, no virus control, combined *KCNJ6* gRNAs 1, 3, and 6 (CRISPRa) and lentiviral expression (Lenti; $N = 1$ donor, 3 replicates). ***C***, Western blot of iso-CTL, CRISPRa, and Lenti expression of GIRK2 (MW = 49 kDa, red arrow). NaK-ATPase loading control (MW = 198 kDa, red arrow). ($N = 1$ donor, 2 replicates scr-gRNA control, 3 replicates *KCNJ6* gRNAs, no virus control, and lentivirus *KCNJ6* vector.) ***D***, Representative images of isogenic control (iso-CTL) neurons, CRISPRa and Lenti expression ↑GIRK2 neurons stained for TUJ1 (magenta), DAPI (blue), and GIRK2 (green); 100× magnification; scale bar and insets = 10 μm. ***E***, Normalization of GIRK2 puncta μm^2 to TUJ1 μm^2; each point represents a single image; coral, CRISPRa and teal, Lenti [*N* images = CRISPRa: 9 iso-CTL (scr-gRNA control), 16 ↑GIRK2 (*KCNJ6* gRNA); *KCNJ6* lentivirus: 9 iso-CTL (no virus control), 10 ↑GIRK2]. All experiments were carried out in Day 42 *NGN2* neurons.

↑GIRK2) of TUJ1 area (Fig. 1*D–F*). Thus, both CRISPRa- and Lenti-mediated *KCNJ6* expression appeared to increase the levels of GIRK2 protein expression similarly (Fig. 1*C–F*).

We next examined whether higher protein expression led to an increase in GIRK current, using whole-cell patch-clamp electrophysiology. Both 553/dCas9-VPR and 12455/Lenti neurons were grown on glass coverslips for 5–6 weeks with HFAs to improve maturation (Johnson et al., 2007; Tang et al., 2013; Odawara et al., 2014). To study GIRK currents, we included 100 µM GTPγS in the internal solution to activate endogenous G-proteins and produce maximal GIRK activation, as previously described (Schreibmayer et al., 1996; Slesinger et al., 1997; Federici et al., 2009). Given that the expression of voltage-gated potassium as well as nonselective ion channels in neurons (Duménieu et al., 2017) can obscure the inward rectification of GIRK channels, we used a GIRK-specific blocker SCH-23390 (referred to as SCH) to assess GIRK current (Kuzhikandathil and Oxford, 2002; Zhao et al., 2020). At ∼5 min following establishment of the whole-cell recording, application of 30 µM SCH rapidly and reversibly inhibited the outward current (Fig. 2*A*). The reversal potential for the SCH-inhibited current was approximately −80 mV (Fig. 2*B*), which is near the calculated equilibrium potential for potassium (E_K; $[K^+]_{out} = 5$ mM, $[K^+]_{in} = 140$ mM), confirming the potassium selectivity of the channel.

Overall, CRISPRa-mediated enhancement and lenti expression of *KCNJ6* led to similar increases in GIRK2 protein (Fig. 1*C–F*); we therefore pooled these data and refer to them as ↑GIRK2. The GIRK current density for SCH-inhibited current was significantly larger in ↑GIRK2 neurons, as compared with isogenic controls (+0.34 pA/pF; $p = 0.028$; $N = 19$ iso-CTL, 23 ↑GIRK2; Fig. 2*E*). Furthermore, ↑GIRK2 neurons exhibited more hyperpolarized resting membrane potentials (−6.7 mV; $p = 0.009$; $N = 29$ iso-CTL, 37 ↑GIRK2; Fig. 1*H*), a larger SCH-induced membrane depolarization (+3.1 mV; $p = 0.016$; $N = 6$ iso-CTL, 13 ↑GIRK2; Fig. 1*I*), and a higher frequency of SCH-induced spontaneous EPSC (sEPSCs; +7.9 Hz; $p = 0.021$; $N = 8$ iso-CTL, 18 ↑GIRK2; Fig. 1*E,F,J*). ↑GIRK2 neurons did not significantly differ in rheobase, suggesting little impact of GIRK2 on action potential thresholds (Extended Data Table 2-1). Additional neuronal properties, including cell capacitance, membrane resistance, or evoked spiking activity revealed no significant differences (Extended Data Table 2-1), indicating preservation of basic cell properties with ↑GIRK2. Collectively, these data support the conclusion that an increase in GIRK channel expression results in a functional increase in GIRK channel activity.

Seven day 17 mM ethanol protocol: transcriptomic evidence of downregulated neuronal maturation and upregulated metabolic activity

Prior to investigating how ↑GIRK2 interacts with ethanol to influence neuronal activity, we first sought to investigate the effect of 17 mM ethanol (equivalent to 0.08% blood alcohol concentration) in iso-CTL neurons over 7 d on gene expression as determined by bulk RNAseq. We used an IEE paradigm, described previously (Scarnati et al., 2020; Popova et al., 2023). For IEE, we supplemented ethanol daily to maintain 17 mM concentration, since the ethanol concentration in the cell culture medium decreases to 5 mM or less after 24 h (Lieberman et al., 2012; Scarnati et al., 2020; Popova et al., 2023). Glutamatergic neurons from four donors were induced in two batches in the absence of astrocytes to provide a pure

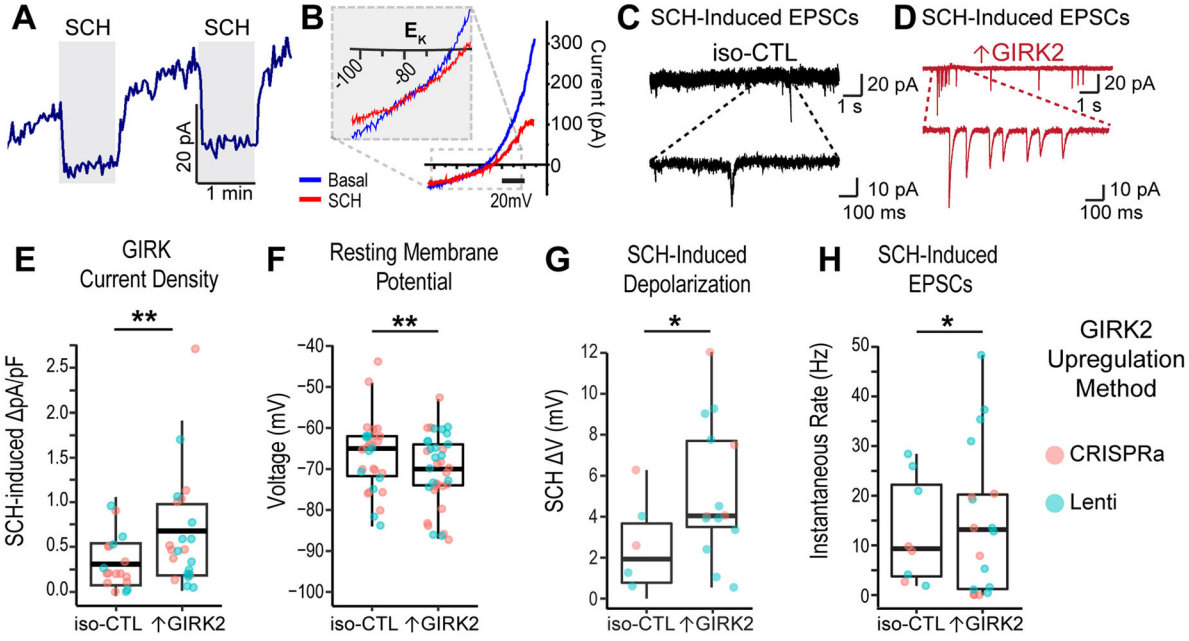

Figure 2. Increased GIRK2 protein expression alters electrophysiology of human glutamatergic neurons. ***A***, Representative traces of GTPγS-activated current with two 1 min pulses of 30 µM SCH-23390 (gray rectangles) voltage-clamped at −40 mV. ***B***, Representative current–voltage curves of basal (blue) and GIRK2-inhibited (SCH-23390, red traces) currents; inset: magnification of current reversal at the potassium equilibrium potential (E_K). ***C***, ***D***, Representative sEPSCs for iso-CTL (black; ***E***) and ↑GIRK2 (red; ***F***) neurons with SCH pulse. Main trace, 10 s; magnified inset, 1 s. ***E–H***, Boxplots showing mean (middle bar), upper and lower quartiles (box), and 1.5 interquartile range (whiskers) of (***E***) SCH-inhibited GIRK current density [pA/pF; $N = 19$ iso-CTL cells (12 scr-gRNA + 7 no virus); 23 ↑GIRK2 (11 CRISPRa + 12 Lenti)]; ***F***, resting membrane potential [$N = 29$ iso-CTL cells (20 scr-gRNA + 9 no virus); 37↑GIRK2 (20 CRISPRa + 17 Lenti)]; ***G***, SCH-induced shift in resting membrane potential [$N = 6$ iso-CTL cells (2 scr-gRNA + 4 no virus); 13 ↑GIRK2 (3 CRISPRa + 10 Lenti)]; and ***H***, instantaneous sEPSC rate (Hz) with SCH [$N = 8$ iso-CTL cells (3 scr-gRNA + 5 no virus); 18↑GIRK2 (7 CRISPRa + 11 Lenti)]. Each point represents a cell; point color indicates GIRK2 expression method (coral, CRISPRa; teal, Lenti). Statistics: GLMM with expression method and batch random effects. $*p < 0.05$, $**p < 0.01$. See Extended Data Table 2-1 for additional patch properties (membrane capacitance, access resistance, rheobase, and action potential threshold).

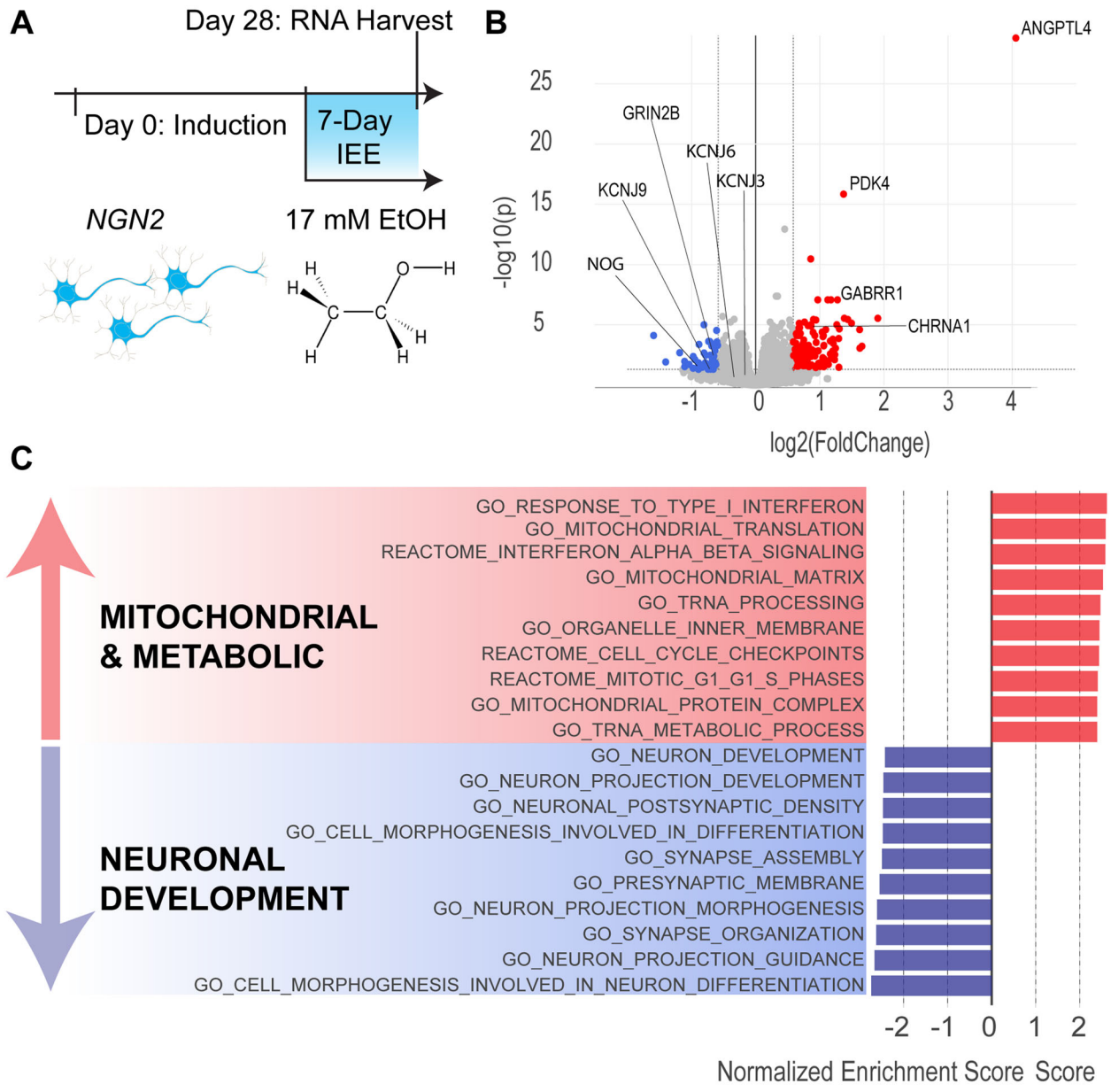

Figure 3. Seven-day IEE increases expression of mitochondrial and metabolic genes and impairs neuronal development genes. ***A***, Timeline for neuronal induction, intermittent 17 mM ethanol exposure, and RNA harvest. ***B***, Volcano plot of DEGs (fold-change = 1.5 and *p* value = 0.05 cutoffs). Blue dots represent downregulated genes and red dots represent upregulated genes. ***C***, GO categories of DEGs. Bars depict normalized enrichment score for each category. See Extended Data Table 3-1 for complete list of significant DEGs. *N* = 4 donors, 2 batches, 4 replicate wells.

neuronal population for RNAseq analyses. At Day 21 postinduction, when neurons begin to be electrically active (Ho et al., 2016), we treated half of the cultures with the IEE protocol for 7 d (on D21) and harvested the neurons at Day 28 postinduction (Fig. 3*A*).

Differential gene expression analysis revealed that 7 d IEE resulted in 127 upregulated and 50 downregulated genes, with Benjamini–Hochberg adjusted *p* value cutoff of 0.05 and fold-change cutoff of 1.5 (Fig. 3*B*; Extended Data Table 3-1). Among them, *PDK4* and *ANGPTL4* showed the largest increase in fold-change. These two genes are involved in regulating the switch between glycolysis and fatty acid oxidation (La Paglia et al., 2017; Ma et al., 2019) and are both influenced by upstream proliferator-activated receptor-γ (PPARγ; Cippitelli et al., 2017; La Paglia et al., 2017). Interestingly, *PDK4* overexpression is associated with loss of metabolic flexibility and promotes excessive transport of calcium into mitochondria (Zhang et al., 2014; Ma et al., 2019; Jeon et al., 2020). Gene ontology (GO) analysis shows the robust upregulation of the associated biological processes (Fig. 3*D*). Most enriched categories are associated with metabolic, mitochondrial, and inflammatory pathways, suggesting one of the impacts of 7 d IEE is on energy utilization in glutamatergic neurons.

Furthermore, GO analysis revealed a significant depletion of differentially expressed genes (DEGs) involved in neuronal development, morphogenesis, and synapse organization—including neurodevelopmental gene *NOG*, voltage-gated potassium channel subunit *KCNH1*, inwardly rectifying potassium channel subunit *KCNJ9*, and ionotropic glutamate receptor subunit *GRIN2B* (Fig. 2*D*, Extended Data Table 2-1). Expression of other inwardly rectifying potassium channels, including *KCNJ6* (GIRK2) and *KCNJ3* (GIRK1), and other canonical markers

of glutamatergic identity, such as glutamate transporter *SCLA17A7* (vGLUT1) and glutamate receptor *GRIA4* (AMPAR), was not significantly affected. Interestingly, several genes involved in inhibitory neurotransmission were upregulated, including *CHRNA9* and *GABRR1* (Fig. 2*C*). Taken together, these data show that 7 d IEE promotes significant alterations in the transcriptome of glutamatergic neurons, indicating the presence of metabolic stress and perturbations in glutamatergic neuronal maturation.

GIRK2 expression counteracts hyperactivity induced by prolonged (7–21 d) 17 mM ethanol exposure

We hypothesized that ↑GIRK2 and IEE would act in concert to inhibit neuronal activity, because of ethanol-induced downregulation of neuronal maturation genes and the direct activation of GIRK channels (Bodhinathan and Slesinger, 2014). To address this, we first used MEAs to measure neuronal local field potentials over weeks of ethanol exposure. Using 553/dCas9-VPR and 12455/Lenti neurons, we followed the same 17 mM IEE paradigm used in bulk RNAseq, starting the protocol at Day 21, 2 weeks after the start of ↑GIRK2 expression (Fig. 4*A*). To track the effects of ethanol exposure and GIRK2 expression levels on the developmental time course, we extended IEE duration beyond 7 d and collected MEA data at Days 28, 35, and 42 (corresponding with 1, 2 and 3 weeks, respectively, of IEE). To maximize consistency of measurements across the multiweek experiment, MEA recordings were collected at the same time of day, ∼24 h after the last supplementation of ethanol, at a time when ethanol was ∼5 mM in the culture medium (Scarnati et al., 2020; Fig. 4*B*).

At day 28, MEA recordings showed very low levels of activity for both groups (Fig. 4*C*). At Days 35 and 42, however, IEE iso-CTL neurons exhibited a 1.49 Hz increase in weighted mean firing rate (WMFR; Fig. 4*D*; $p = 0.01$) and an 0.95 Hz increase in WMFR (Fig. 4*E*; $p = 0.04$), respectively. In contrast, ↑GIRK2 neurons appeared unaffected by 2 weeks of IEE at Day 35 (Fig. 4*C*) but were significantly inhibited after 3 weeks of IEE at Day 42, with a statistically significant interaction effect between increased GIRK2 expression and ethanol exposure (−1.37 Hz WMFR; $p = 0.02$; Fig. 4*E*).

GIRK2-upregulated neurons show inhibited spontaneous calcium spiking activity after 21 d IEE

To investigate the combined effects of 21 d IEE and ↑GIRK2 on glutamatergic neuronal activity under ethanol-free conditions, we conducted Ca^{2+} imaging, using Ca^{2+} transients as a proxy for neuronal activity. We expanded our donor pool to five cell lines (CRISPRa: 553/dCas9-VPR and 2607/dCas9-VPR; Lenti: 12455, 9429, and BJ) and carried out the same IEE protocol with *NGN2*-induced glutamatergic neurons, as described for the MEA experiments (Fig. 4*A*). Ca^{2+} transients were detected with Fluo4-AM and were baseline-corrected, filtered for non-neuronal events, and deconvolved to quantify peak frequency and height (Fig. 5*A–C*; $N = 50–200$ ROIs|5 donors|3 replicates; see Extended Data Table 5-1 for all ROI N values for each replicate experiment). Neurons without spontaneous activity were excluded from spontaneous activity analysis.

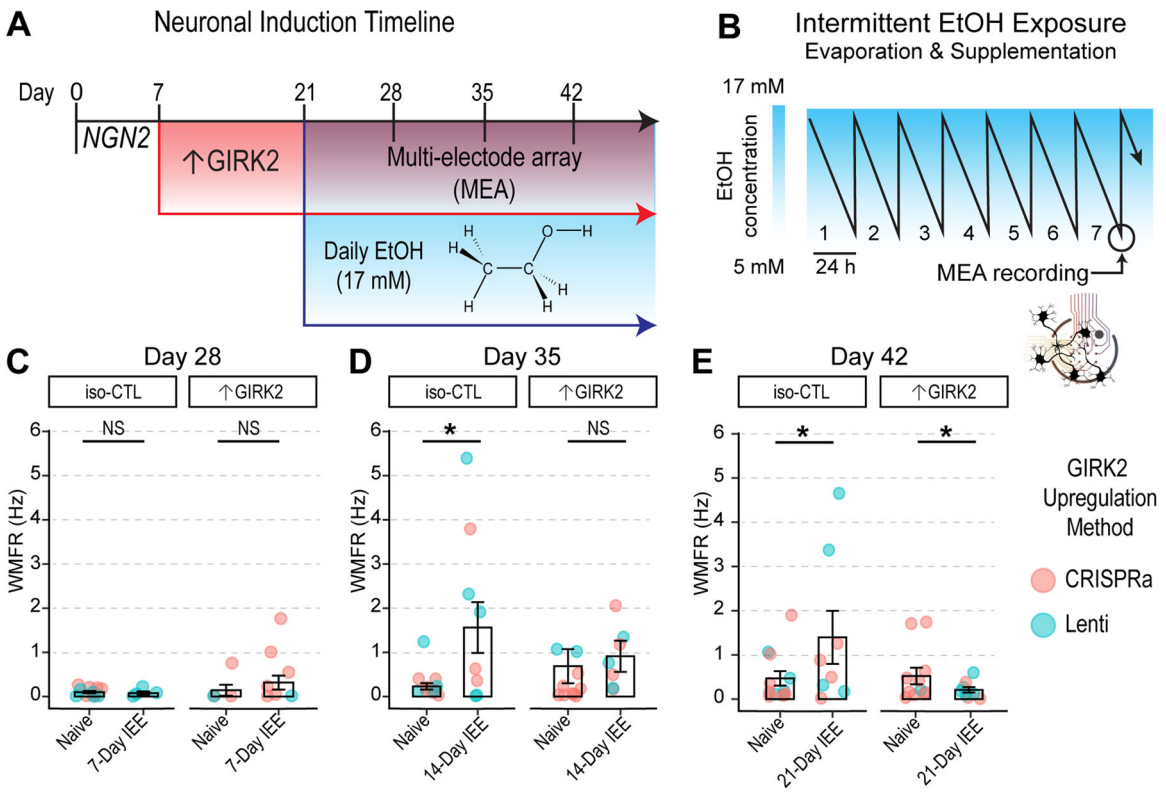

Figure 4. Increased GIRK2 expression counteracts hyperactivity induced by low-ethanol conditions. ***A***, Timeline of neuronal differentiation, GIRK2 upregulation, and ethanol exposure. ***B***, Schematic of 7 d IEE, showing change in ethanol concentration over 24 h due to evaporation (Scarnati et al., 2020; Popova et al., 2023). ***C–E***, Neuronal firing rates (WMFR) measured with MEA is shown for *NGN2* neurons at Days 28 (1 week ethanol; ***C***), 35 (2 weeks ethanol; ***D***), and 42 (3 weeks ethanol; ***E***); each point represents an MEA well; $N = 2$ donors|5 batches. Point color indicates GIRK2 expression method (coral, CRISPRa; teal, Lenti). GLMM includes batch and donor random effects. $^*p < 0.05$.

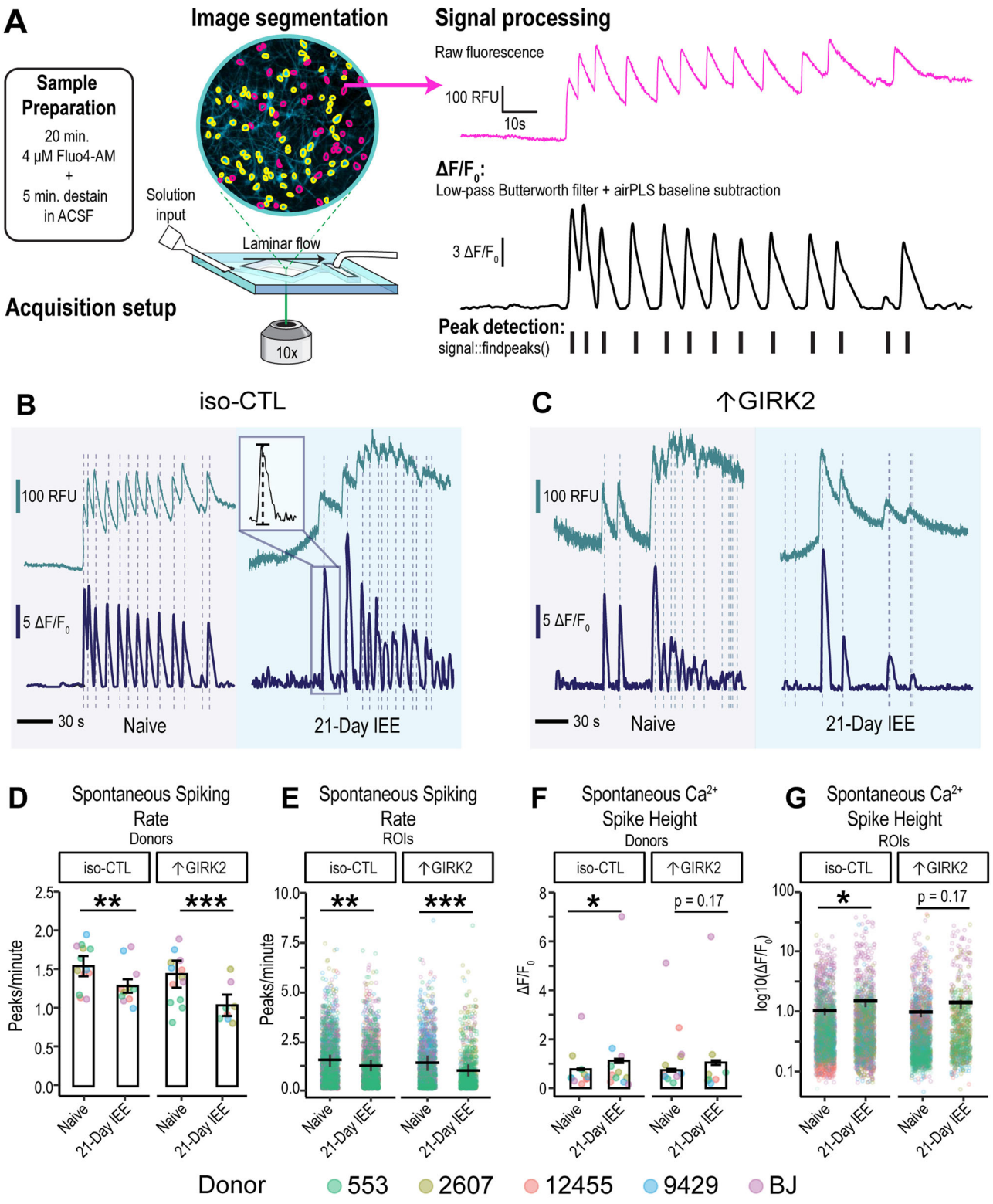

Figure 5. Combined effect of 21 d IEE and ↑GIRK2 expression inhibits spontaneous activity of excitatory neurons. ***A***, Schematic representation of calcium imaging experimental and analysis procedure, including sample preparation, acquisition setup, and signal processing. ***B–D***, Representative fluorescence traces showing Ca^{2+} spikes in alcohol-naive (gray background) and 21 d IEE-treated (blue background) iso-CTL (***B***) and ↑GIRK2 (***C***) excitatory neurons on D42. Inset in iso-CTL: zoom of Ca^{2+} spike illustrating peak height measurement. Vertical dashed lines indicate auto detection of Ca^{2+} peaks. Top trace is raw fluorescence. Bottom trace is baseline-corrected $\Delta F/F_0$. Scale bars = 100 RFU, 5 $\Delta F/F_0$, and 30 s. See Extended Data Figure 4-1 for schematic of Ca^{2+} fluorescence acquisition and processing pipeline. ***D***, ***E***, Ca^{2+} spike rate (peaks/minute) plotted as an average for each donor replicate ($n = 5$ donors, 3 replicates; ***D***) and as individual neuronal ROIs (see Extended Data Table 5-1 for complete list of spontaneously active neuronal ROI Ns for each replicate experiment; ***E***). ***F***, ***G***, Ca^{2+} transient height ($\Delta F/F_0$) plotted as an average for each donor replicate (***F***) and individual ROIs (***G***). Color indicates donor (coral, 12455; dark yellow, 3440; green, 553; blue, 9429; and purple, BJ). GLMM includes replicate and donor random effects. $*p < 0.05$, $**p < 0.01$, $***p < 0.001$.

Similar to MEA findings, IEE for 21 d significantly reduced the frequency of calcium spiking in spontaneously active neurons in ↑GIRK2 neurons in ethanol-free solution (decrease of −0.51 peaks/minute, $p < 0.00001$ IEE effect in ↑GIRK2 neurons; $p = 0.0006$ interaction ↑GIRK2:IEE; Fig. 5*D*,*E*). One interpretation of this finding is that the inhibitory interaction of IEE with ↑GIRK2 is not caused by a direct interaction of ethanol on GIRK2 channels. In contrast to MEA results, iso-CTL neurons exhibited decreased spontaneous Ca^{2+} activity as a result of IEE under ethanol-free conditions, albeit to a lesser extent than ↑GIRK2 neurons (−0.19 peaks/min; $p = 0.003$; Fig. 5*D*,*E*). IEE iso-CTL neurons also displayed a significant increase in calcium transient peak heights (+0.33 $\Delta F/F_0$; $p = 0.002$; Fig. 5*F*,*G*), possibly indicating stronger depolarization. ↑GIRK2 neurons, on the other hand, showed no significant change in Ca^{2+} levels (+0.16 $\Delta F/F_0$; $p = 0.10$), suggesting that ↑GIRK2 expression ablates ethanol-induced increases in intracellular Ca^{2+}.

GIRK2 expression interacts with ethanol to differentially regulate glutamate response and intrinsic excitability

We hypothesized that, in addition to inhibiting spontaneous activity, 21 d ethanol exposure would alter neuronal excitability in ↑GIRK2 neurons. We interrogated neuronal excitability by rapid bath application of glutamate (10 μM for 30 s), which would be expected to depolarize neurons and elicit Ca^{2+} spikes. We measured the proportion of glutamate-responsive neurons, the number of Ca^{2+} peaks, the latency to the first spike, and Ca^{2+} peak height (Fig. 6*C*). In iso-CTL neurons, 21 d IEE increased the proportion of glutamate-responsive neurons (+13.3%, $p < 0.001$; $N = 1{,}203$–$2{,}609$ ROIs/group; see Extended Data Table 6-1 for full list of ROI N values for each donor and replicate; Fig. 6*D*). In the glutamate-active subset of neurons, IEE also increased the number of glutamate-evoked spikes (+0.2 spikes, $p = 0.02$; Fig. 6*A*,*E*). These effects of IEE were absent in ↑GIRK2 neurons (Fig. 6*B*,*D*,*E*). Furthermore, IEE decreased latency to first spike with glutamate (Fig. 6*C*) in iso-CTL neurons, suggesting an increase in response to glutamate and/or excitability (−3.4 s, $p < 0.00001$; Fig. 6*F*). In contrast, 21 d IEE ↑GIRK2 neurons increased their latency to first spike with glutamate (+2.1 s, $p = 0.0312$ exposure effect; $p < 0.00001$ interaction effect; Fig. 5*F*).

To further validate of latency calculation, we examined the latency to the first spike with a random 30 s epoch in the same neuron. The average latency to the first spike was 14.7 ± 0.3, 15.1 ± 0.3, 15.2 ± 0.3, and 16.0 ± 0.4 for naive iso-CTL, 21 d IEE iso-CTL, naive ↑GIRK2, and 21 d IEE-↑GIRK2 groups, respectively; p values equal to 0.92 and 0.39 for the impact of IEE on iso-CTL and ↑GIRK2 neurons, respectively. In contrast, the latency to the first spike seen with glutamate application was 4.7 ± 0.2, 4.6 ± 0.2, 4.1 ± 0.2, and 4.4 ± 0.4 for each treatment group, as listed above, confirming the latency to the first spike reflects a response to glutamate.

Similar to the measurements of spontaneous activity (Fig. 5*F*,*G*), calcium peak heights were significantly larger in IEE iso-CTL neurons (+0.36 $\Delta F/F_0$; $p = 3 \times 10^{-6}$). This increase was not observed in ↑GIRK2 neurons (Fig. 6*G*). Taken together, these data indicate that 21 d IEE heightens glutamate receptor activity and/or excitability in iso-CTL neurons, whereas ↑GIRK2 neurons exhibit diminished glutamate responses.

To determine whether differences in glutamate-responsive neurons were due to changes in glutamate sensitivity or in intrinsic excitability, we bath-applied 15 mM KCl in ACSF to directly depolarize the neurons (15 mM KCl is predicted to produce a ∼32 mV positive shift in the resting membrane potential) and measured Ca^{2+} spikes in the same population of glutamate-responsive neurons. As before, Ca^{2+} flux was elevated in 21 d IEE iso-CTL neurons (+0.23 $\Delta F/F_0$, $p < 1 \times 10^{-6}$), while ↑GIRK2 neurons were unaffected (Fig. 5*J*). However, 21 d IEE in ↑GIRK2 neurons increased proportion of KCl-responsive ROIs (+8.3%, $p = 0.009$ IEE effect; $p < 1 \times 10^{-6}$ interaction effect; Fig. 5*H*) and number KCl-evoked Ca^{2+} spikes (+0.54 spikes, $p < 1 \times 10^{-6}$; Fig. 5*I*). Iso-CTL neurons, conversely, had a lower proportion of KCl-responsive ROIs (−16.5%, $p < 1 \times 10^{6}$; Fig. 5*H*) and no difference in number of evoked spikes ($p = 0.4$; Fig. 5*I*). These data indicate that, unlike glutamate-evoked activity, depolarization-evoked activity is suppressed in iso-CTL neurons and heightened in ↑GIRK2 neurons following 21 d IEE.

To further probe potential differences in intrinsic excitability, we examined the maximum number of spikes induced with depolarizing current injection steps (20 pA) using whole-cell patch-clamp electrophysiology (Fig. 6*K*). Similar to KCl-induced firing (Fig. 6*I*), there was no significant difference in the number of spikes for iso-CTL neurons with 21 d IEE. In contrast, we recorded a higher number of spikes in ↑GIRK2 neurons with 21 d IEE (+2.8 spikes, $p = 0.002$; Fig. 5*K*,*L*), similar to that with KCl-induced firing. Taken together, these results suggest inhibitory effects of ↑GIRK2 with 21 d IEE appear to be specific to glutamate-mediated activity.

To investigate potential molecular mechanisms underlying combined effects of increased GIRK2 expression and IEE on glutamatergic function, we performed bulk RNAseq differential gene expression analysis in the same cohort of neurons subject to 21 d IEE. Acting in concert, ↑GIRK2 and IEE impacted expression of multiple genes essential for synaptic function (Fig. 7, Extended Data Table 7-1). In contrast to untreated isogenic controls, neurons treated with IEE +↑GIRK2 exhibited downregulation of glutamatergic receptor (*GRIA1*, *GRIN1* ,and *GRIN2B*) and potassium channel (*KCND2* and *KCNJ3*) genes (Fig. 7*A*). This transcriptomic landscape is consistent with the decreased response to glutamate and increased membrane excitability in IEE + ↑GIRK2 neurons (Fig. 6). Furthermore, the combination of IEE and ↑GIRK2 led to downregulation of Ca^{2+} signaling genes, including the voltage-gated Ca^{2+} channel *CACNAD1* and intracellular Ca^{2+}-binding protein *CALB2* (Fig. 7*A*). Reduced expression of Ca^{2+}-sensitive genes may reflect an active process in ↑GIRK2 neurons working in opposition to IEE-induced increases in intracellular calcium present in isogenic controls both during spontaneous (Fig. 5) and evoked (Fig. 6) neuronal activity.

To gain insight into how these shifts in RNA expression may contribute to specific biological processes involved in neuronal signaling, we analyzed synaptic GO using the SynGO online portal (Koopmans et al., 2019; Fig. 7*B*; Extended Data Table 7-2). While each of the main biological processes was significantly impacted by combined ↑GIRK2 and IEE (i.e., pre- and postsynaptic function, signaling, transport, organization, and metabolism), presynaptic pathways were the most affected (Fig. 7). Specifically, regulation of presynaptic Ca^{2+} levels and Ca^{2+}-dependent vesicle fusion (both involving *CACNA1B*) appeared especially sensitive to combined ↑GIRK2 and IEE (Fig. 7). These alterations in presynaptic regulatory mechanisms occurred in conjunction with changes in synapse assembly, synaptic translation, and dendritic transport. Taken together, these data support an active transcriptomic process underlying the observed changes in neuronal activity (e.g., altered glutamate

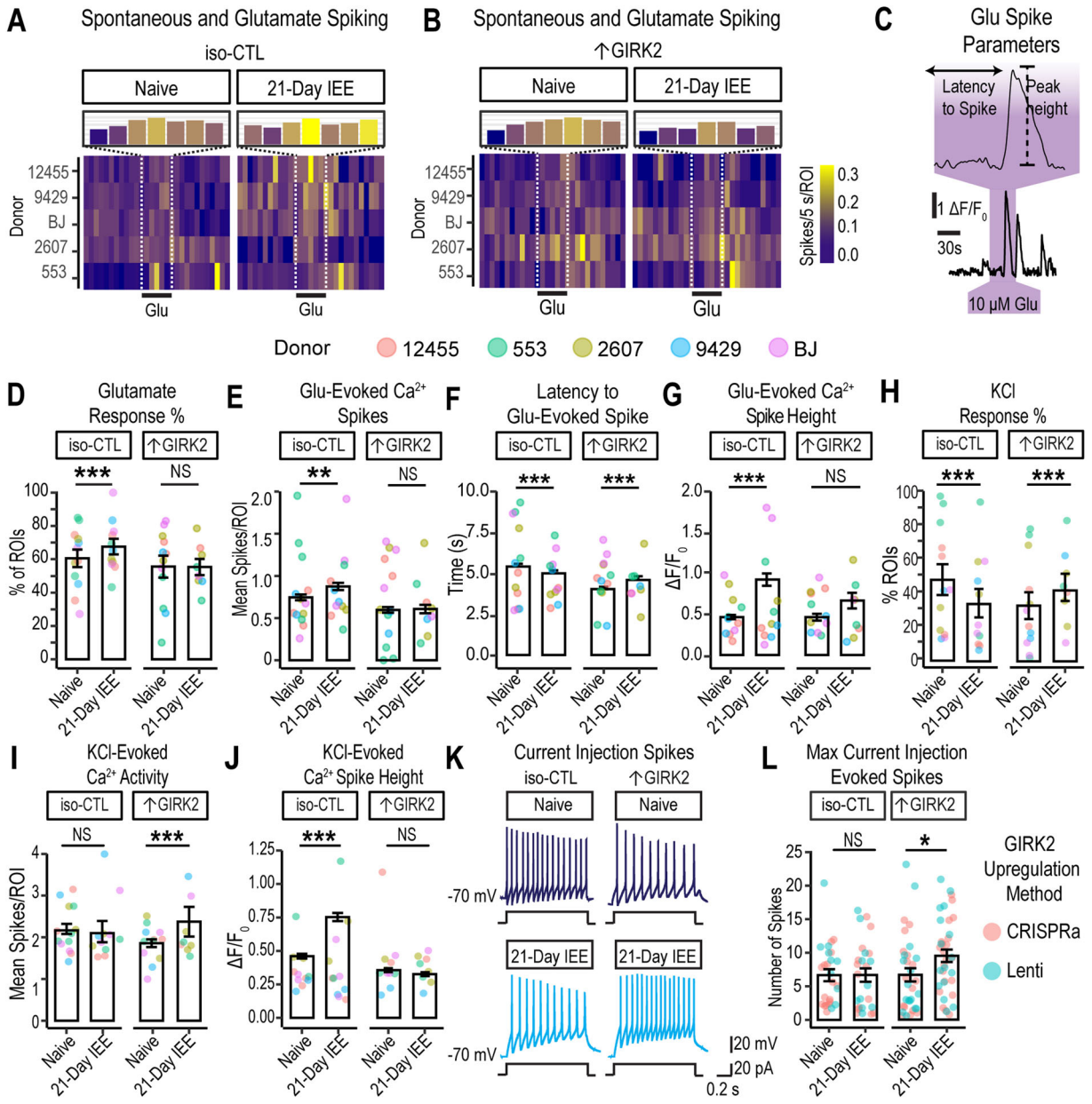

Figure 6. Increased GIRK2 expression and IEE impact glutamate response and membrane excitability in glutamatergic neurons. ***A***, ***B***, Calcium spiking activity heatmap for iso-CTL (***A***) and ↑GIRK2 (***B***) neurons, either naive and with 21 d IEE. Five-second bins, normalized to number of cells (spikes/5 s/ROI). Inset magnification shows number calcium spikes/5 s/ROI during the 30 s pulse of 10 μM glutamate. Color gradient indicates activity intensity (violet-blue, low; yellow, high). ***C***, Example deconvolved Ca^{2+} fluorescence trace and latency to spike with a 30 s glutamate pulse. ***D***, Percentage of excitatory neurons responsive to 30 s glutamate pulse (10 μM). (See Extended Data Table 6-1 for complete list of all active neuronal ROI Ns for each replicate experiment.) ***E***, Number of calcium spikes during each 30 s glutamate pulse (see Extended Data Table 6-2 for complete list of all glutamate-responsive ROI Ns for each replicate experiment). ***F***, Latency to spike (s) in response to 30 s glutamate, pulse (10 μM). ***G***, Calcium peak height ($\Delta F/F_0$) evoked by glutamate for iso-CTL and ↑GIRK2 neurons, either ethanol-naive or with 21 d IEE. ***H***, Percentage of ROIs responsive to 15 mM KCl. ***I***, Number of spikes evoked by 1 min 15 mM KCl pulse. ***J***, Ca^{2+} spike height during 1 min 15 mM KCl ($\Delta F/F_0$). KCl ($N = 1{,}203$–$2{,}608$ ROIs/group). Point color indicates donor (coral, 12455; dark yellow, 2607; green, 553; blue, 9429; and purple, BJ; see Extended Data Table 6-3 for complete list of glutamate-responsive and KCl-active ROI Ns for each replicate experiment). ***K***, Representative action potentials evoked by 1 s current injection step (20 pA) in naive and 21 d IEE iso-CTL and ↑GIRK2 neurons. ***L***, Maximum number of evoked spikes measured in current-clamp with 20 pA current injection steps from holding potential of approximately −70 mV (N = iso-CTL: 26 naive, 25 21 d IEE; ↑GIRK2: 33 naive, 37 21 d IEE). Point color indicates upregulation method (coral, CRISPRa; teal, Lenti). GLMM includes batch and donor effects. $*p < 0.05$, $**p < 0.01$, $***p < 0.001$.

response, intrinsic excitability, and intracellular calcium handling) resulting from the dual effects of ↑GIRK2 and IEE.

Impact of ethanol exposure, GIRK2 expression, and glutamate on mitochondrial function in excitatory neurons

SynGO analysis (Fig. 7*B*, Extended Data Table 7-2) indicated adaptations in metabolic processes involved in translation at the synapse—an integral aspect of activity-dependent modulation of neuronal circuitry. Furthermore, transcriptomic analysis in Day 28 neurons following 7 d IEE (Fig. 3*D*) suggested that metabolic and mitochondrial alterations is an early response to ethanol, preceding significant changes to glutamatergic signaling. Together, these suggested a role for mitochondria with chronic alcohol use (Vandecasteele et al., 2001; Cassano et al., 2016; Walter et al., 2017; Giorgi et al., 2018; Verma et al., 2022).

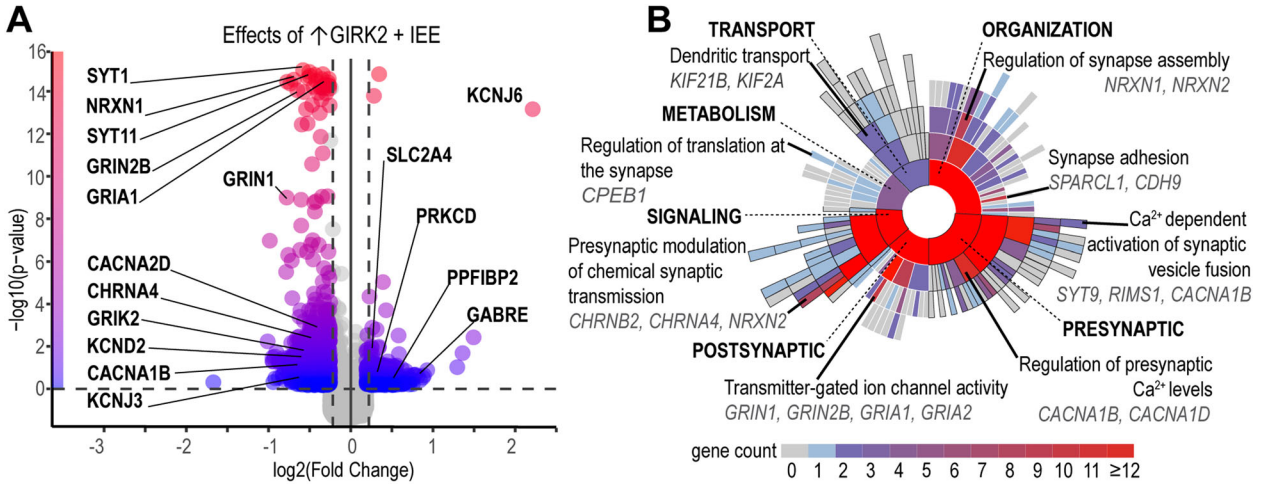

Figure 7. Intermittent ethanol 21 d exposure combined with ↑GIRK2 expression uniquely impacts synaptic function gene pathways. ***A***, Volcano plot of differentially regulated genes (1.25 log2 fold-change and 0.05 *p* value cutoffs) as a result of the combined effect of IEE and ↑GIRK2 on iso-CTL neurons. Color gradient indicates −log10 (*p* value), with blue, 0, and red, 16. Select neuronal excitability genes highlighted—see Extended Data Table 7-1 for full list of differentially regulated synaptic function transcripts resulting from combined↑GIRK2 and 21 d IEE. ***B***, Sunburst plot of SynGO annotated GOs, including synaptic transport, metabolism, organization, signaling, presynaptic, and postsynaptic biological processes. Color indicates number of genes enriched in each pathway, including child terms (gray, 0; blue, 1; red, ≥12). Top enriched pathways and DEGs are highlighted for each biological process. See Extended Data Table 7-2 for complete list of annotated SynGO pathways and their enrichment values. $N = 2$ donors CRISPRa, 4 donors Lenti|2 batches|3 technical replicates/donor/batch.

We therefore investigated the effect of IEE and ↑GIRK2 on the developmental time course of mitochondrial function in glutamatergic neurons. We hypothesized that ↑GIRK2 would prevent changes in cellular respiration caused by 7 and 21 d IEE, similar to the mitigating effect on increased calcium activity. To test this prediction, we utilized the mitochondrial stress test (Agilent Technologies Seahorse assay) with monocultures of glutamatergic neurons (monocultures eliminate the potential confound of glial cells). Respiration was measured in ethanol-free conditions at Day 28 postinduction with 7 d IEE and at Day 42 with 21 d IEE ($N = 5$ donors|4 wells|3 batches/timepoint) and normalized for cell density. Seven-day IEE resulted in significant impairment of basal (−17.5 pmol/min/cell OCR; $p = 0.03$; Fig. 8*A*,*C*) and maximal (−72.6 pmol/min/cell OCR; $p = 0.04$; Fig. 8*A*,*D*) cellular respiration in iso-CTL neurons. In contrast, ↑GIRK2 neurons appeared less sensitive to IEE (−10.5 pmol/min/cell OCR; $p = 0.61$). This decrease in respiration in IEE iso-CTL neurons may be the stimulus for upregulation of mitochondrial and metabolic genes as measured in RNAseq (Fig. 3*D*), serving as a potential compensatory mechanism.

At Day 42, the overall OCR was higher than at Day 28 (Fig. 8*A*–*F*), reflecting a parallel between increased neuronal activity (Fig. 4*C*–*E*) and increased oxygen consumption. Twenty-one-day IEE significantly increased oxygen consumption during basal (+352 pmol/min/cell OCR; $p = 0.0006$; Fig. 8*E*) and maximal (+928 pmol/min/cell OCR; $p = 0.00003$; Fig. 8*F*) respiration in iso-CTL neurons. Notably, ↑GIRK2 neurons did not show the increase in basal or maximal respiration with 21 d IEE (Fig. 8*B*). Statistical analysis indicates an interaction between ↑GIRK2 and ethanol exposure for both basal ($p = 0.02$; Fig. 8*E*) and maximal ($p = 0.009$; Fig. 8*F*) respiration. These results suggest a degree of resilience and potential pro-allostatic influence from ↑GIRK2.

To test whether these changes were reflective of activity-dependent energy demands, we stimulated neuronal activity with an acute injection of 10 µM glutamate and measured ATP-linked respiration (Fig. 9*A*,*B*). At Day 28, we observed no differences in ATP-linked respiration at basal levels of activity, regardless of ethanol exposure or GIRK2 expression levels (Fig. 9*C*). The glutamate (10 µM) challenge, on the other hand, reduced ATP-linked respiration in IEE iso-CTL (−66.3 pmol/min/cell OCR; $p = 0.017$) but not in ↑GIRK2 neurons ($p = 0.49$; Fig. 9*C*). This suggests an initial impairment in the ability of iso-CTL neurons to meet activity-dependent energy demands, which are likely lessened by ↑GIRK2 expression.

At day 42, iso-CTL neurons exhibited a surge in ATP-linked respiration (+260 pmol/min/cell OCR; $p = 0.03$; Fig. 9*B*,*D*) under basal conditions, consistent with the observed increases in basal (Fig. 8*E*) and maximal (Fig. 8*F*) OCR. Interestingly, the glutamate (10 µM) challenge eliminated these effects, boosting respiration in ethanol-naive neurons and dampening respiration in ethanol-exposed iso-CTL neurons. Since ethanol exposure increases glutamate sensitivity and firing in iso-CTL neurons, these findings support the conclusion of increased energy demands and the involvement of compensatory mechanisms. In line with the reduced glutamate response evident in Ca^{2+} imaging (Fig. 6*B*,*D*–*G*), ATP-linked respiration remained unchanged in ↑GIRK2 neurons following 21 d IEE ($p = 0.57$; Fig. 9*B*,*D*).

Overall, these transcriptomic and functional data support our observations of increased GIRK2 moderating the IEE-induced mitochondrial respiratory alterations. Mitochondrial stress tests data represent a progression from an initial impairment to a subsequent surge of mitochondrial function as a result of prolonged ethanol exposure. Our findings also suggest that ethanol exposure confers a metabolic challenge, which is exacerbated by the presence of elevated glutamate. Increased GIRK2 expression appears to prevent this trajectory, as evidenced by unaltered cellular respiration regardless of ethanol exposure or glutamate challenge. Further investigation of mitochondrial localization, integrity, and neuronal metabolome is needed to parse the precise role of increased GIRK2 on metabolic adaptations to ethanol exposure in excitatory neurons.

Discussion

In the current study, we employed an isogenic approach to directly examine the functional effects of GIRK2 channels in

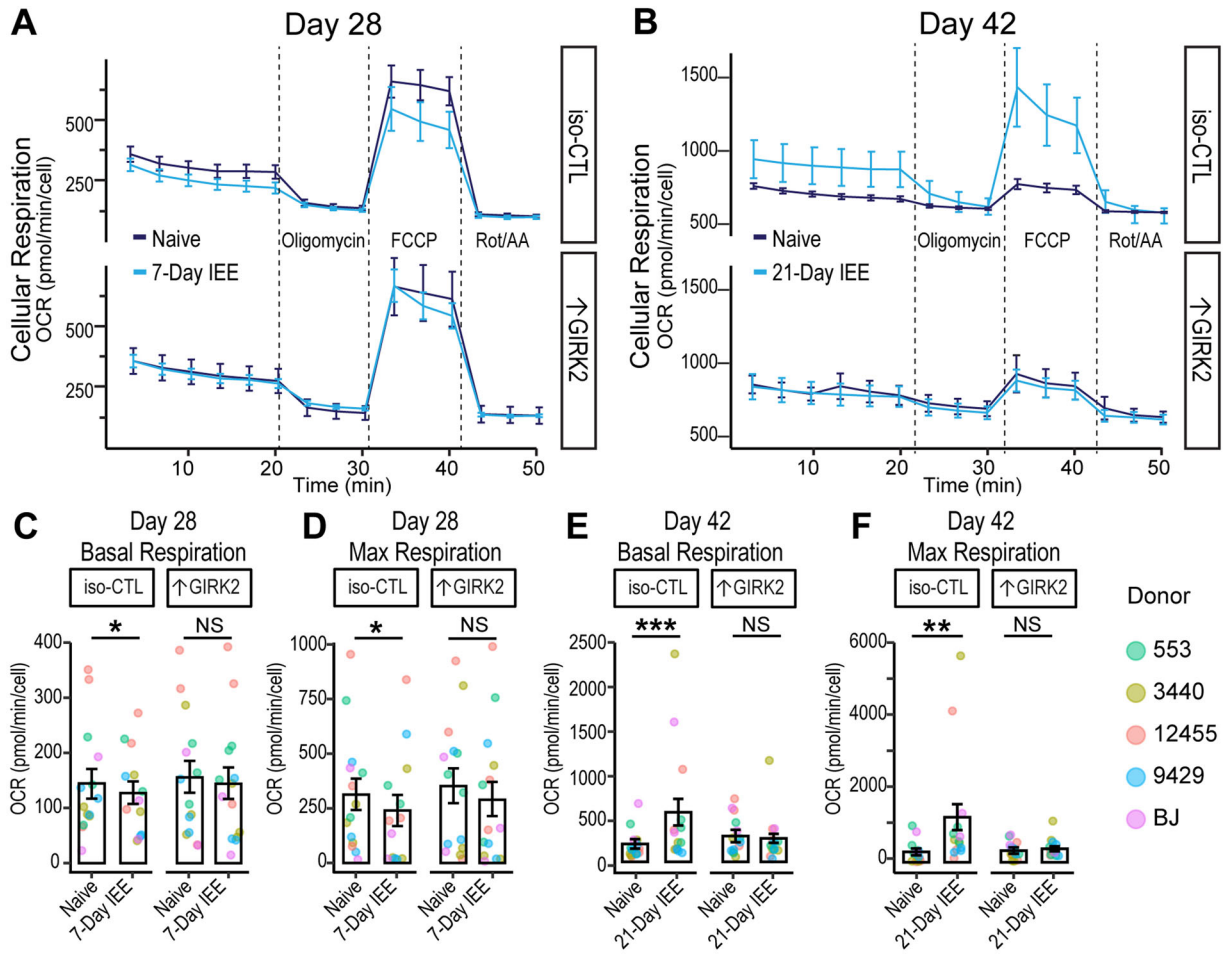

Figure 8. ↑GIRK2 expression counteracts effects of IEE on mitochondrial function. ***A***, ***B***, Time course of cell density-normalized OCR (pmol/minute/cell) during the mitochondrial stress test in CTL and ↑GIRK2 neurons at Day 28 (7 d IEE; ***A***) and Day 42 (21 d IEE; ***B***) postinduction. Line color indicates ethanol exposure: dark blue, naive; light blue, IEE. ***C–F***, Day 28 postinduction basal (***C***) and maximal OCR (pmol/min/cell; ***D***) and D42 basal (***E***) and maximal (***F***) OCR in WT and ↑GIRK2 neurons naive to ethanol or with IEE. *$p < 0.05$, **$p < 0.01$, ***$p < 0.001$.

human excitatory glutamatergic neurons and to investigate their role in adaptations to physiological concentrations of ethanol over 21 d. We hypothesized that increases in GIRK2 expression would impact neuronal response to ethanol exposure, either through direct interaction with the alcohol-binding pocket in GIRK2 or through secondary mechanisms and regulation of neuronal excitability. We found that increased GIRK2 expression (↑GIRK2) mitigates changes in neuronal activity and mitochondrial respiration induced by 21 d intermittent 17 mM ethanol exposure.

Human neurons with ↑GIRK2 exhibited more hyperpolarized resting potentials, and larger GIRK-like currents (SCH-inhibited), as expected for expression of an inwardly rectifying potassium channel (Kuzhikandathil and Oxford, 2002; Lüscher and Slesinger, 2010; Zhao et al., 2020). A major finding was that several of the changes in spontaneous neuronal activity induced by IEE (including increased MEA firing and increased amplitude of Ca^{2+} transients) were absent in ↑GIRK2 neurons, suggesting a mitigating effect of increased GIRK2. We explored whether these changes occurred through differences in glutamate response or intrinsic excitability, uncovering changes in both excitability and suppression of IEE-induced increase in glutamate sensitivity with ↑GIRK2 expression. The increase in neuronal activity with glutamate (i.e., increased % of responsive neurons, decreased latency to spike, and increased number of spikes/glutamate pulse) following IEE was blunted by ↑GIRK2.

Transcriptomic data suggested that IEE-induced increase in glutamate responsiveness for iso-CTL neurons was not attributable to changes in glutamate receptor expression, implicating processes downstream of RNA, such as phosphorylation and ubiquitination regulation of receptor trafficking, surface expression, and turnover (Desch et al., 2021; Warner et al., 2022). Combination of 21 d IEE with ↑GIRK2 neurons reduced expression of NMDAR subunits 1 and 2B and AMPAR subunit 1, possibly reflecting transcriptomic compensation for altered glutamate sensitivity. Furthermore, synaptic GO analysis indicated a role for GIRK2 in presynaptic mechanisms contributing to glutamatergic adaptations to IEE. Specifically, differential regulation of voltage-gated Ca^{2+} channel subunits (including *CACNA1B*, *CACNA2D*) and synaptotagmin family members (including *SYT1*, *4*, *5*, *7*, and *11*) points to calcium-mediated vesicle release as a major consequence of combined ↑GIRK2 and IEE. Additional experiments, such as measuring miniature EPSCs and synaptosome proteomics, are necessary to assess the possible presynaptic changes mediated by IEE and ↑GIRK2 interactions.

Unexpectedly, ↑GIRK2 neurons appeared to be more excitable with depolarization following IEE. This change could result from the decreased potassium channel expression seen in

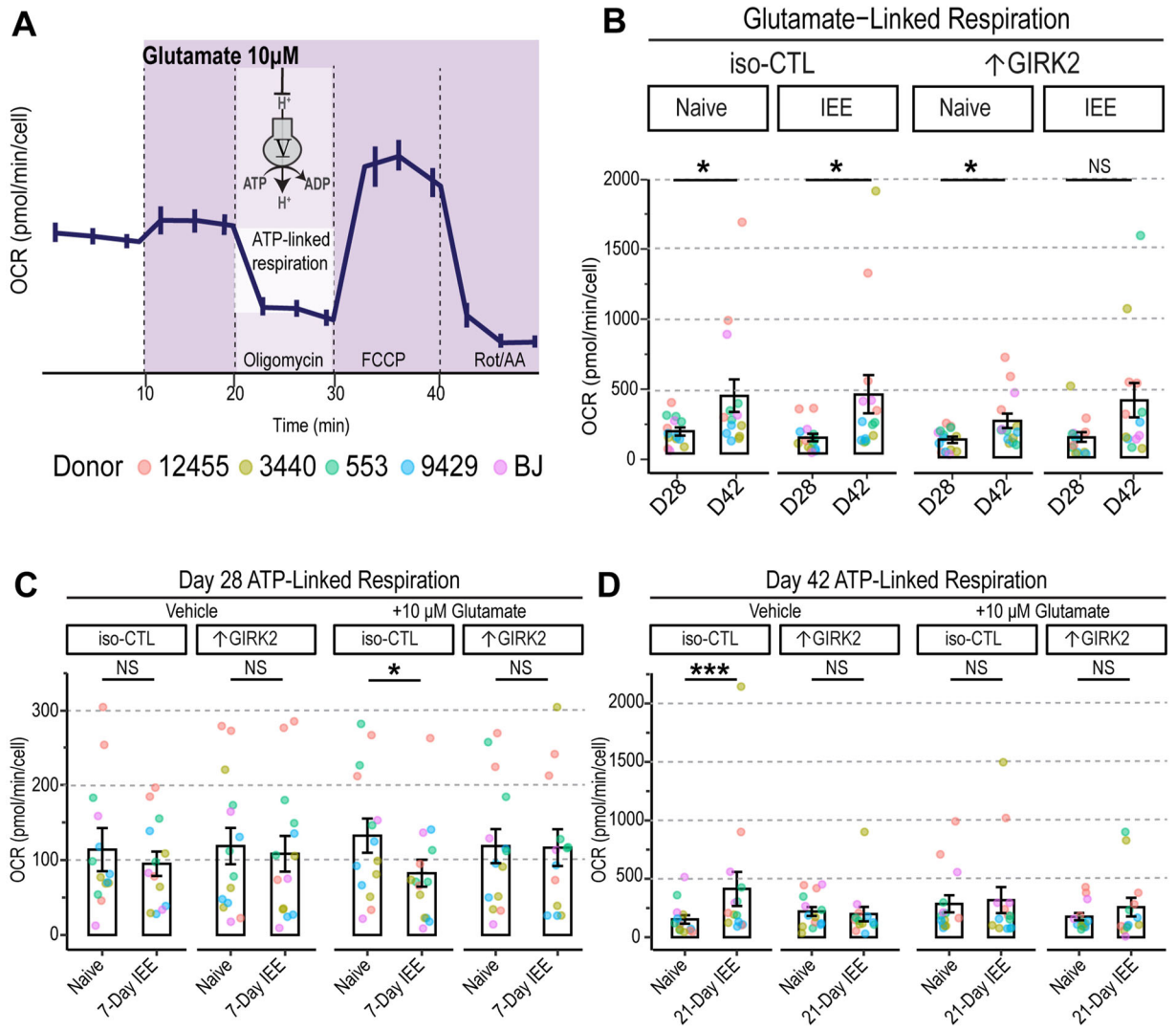

Figure 9. ↑GIRK2 expression counteracts IEE-induced deficit in ATP production in the presence of glutamate. ***A***, Schematic representation of acute 10 μM glutamate injection during the mitochondrial stress test and mechanism of ATP-linked respiration measurement. ***B***, Glutamate linked respiration in iso-CTL and ↑GIRK2 *NGN2* neurons at 28- and 42 d postinduction (D28 and D42, respectively). Each point represents an average of 4 wells from 3 replicate experiments ($N = 5$ donors). ***C***, ***D***, ATP-linked respiration in D28 (***C***) and D42 (***D***) neuron naive to ethanol or with IEE during basal (vehicle) and stimulated (10 μM glutamate) conditions (pmol/min/cell). Each point represents and average of 4 wells from 3 replicate experiments ($N = 5$ donors). Point color indicates donor (coral, 12455; dark yellow, 3440; green, 553; blue, 9429; purple, BJ). GLMM includes donor and batch effects. $*p < 0.05$, $**p < 0.01$, $***p < 0.001$.

RNAseq data. Alternatively, a reduced voltage-dependent inactivation of Na^+ as a consequence of hyperpolarization in ↑GIRK2 neurons with IEE could also increase neuronal excitability (Bähring et al., 2012; Fourcaud-Trocmé et al., 2022; Ransdell et al., 2022). Together, these findings favor the conclusion that the synergistic effect of IEE and ↑GIRK2 expression targets glutamate receptor-dependent signaling. Further investigation is necessary to ascertain the relationship between transcriptomic responses to IEE and corresponding states of protein activity.

Increased GIRK2 expression also prevented increases in the amplitude of calcium peaks induced by IEE in iso-CTL neurons. Intracellular calcium dynamics are multiplex, and the amplitude of calcium peaks could be affected by neuronal firing activity and/or changes in voltage-gated calcium channels. Since elevated intracellular calcium is a hallmark of excitotoxicity (Verma et al., 2022), GIRK2-mediated inhibition in ethanol-exposed glutamatergic neurons may serve a protective role. Consistent with this interpretation, calcium influx through NMDAR channels has been shown to increase surface expression of GIRK channels (Chung et al., 2009), supporting the conclusion that GIRK channel expression is linked to fluctuations in glutamatergic signaling. GIRK channels are also important for synaptic depotentiation (Chung et al., 2009).

In support of our finding that the upregulation of GIRK2 plays an important role in modulating excitability and response to ethanol in human glutamatergic neurons, a recent study found that neurons derived from AUD-diagnosed participants with specific *KCNJ6* SNPs had lower levels of GIRK2 expression, greater neurite area, and heightened excitability as compared with neurons derived from unaffected individuals (Popova et al., 2023). Overexpression of GIRK2 in neurons from AUD-diagnosed individuals mimicked the effects of the 7 d IEE protocol, eliminating differences in neuronal morphology induced excitability (Popova et al., 2023). Thus, in the context of AUD, increased GIRK2 expression and subsequent neuronal inhibition appears to exert a normalizing influence, possibly through regulatory mechanisms of neurotransmitter release and intracellular calcium levels.

Given the impact of increased GIRK2 on intracellular calcium in neurons exposed to ethanol, ↑GIRK2 may also help maintain normal mitochondrial function. Recent work by Sun et al. showed that glutamatergic neurons metabolize ethanol, using it as a preferred energy source over glucose in chronic ethanol exposure conditions (Sun et al., 2023). Mitochondria are vulnerable to ethanol-induced metabolic changes (Tapia-Rojas et al., 2017; León et al., 2022; Lim et al., 2023) and their regulation of calcium homeostasis plays a key role in excitotoxicity (Vandecasteele et al., 2001; Giorgi et al., 2018; Verma et al., 2022). The upregulation of mitochondrial and metabolic genes after 7 d IEE suggests an early metabolic response to ethanol. Furthermore, several groups reported that ethanol exposure of iPSC-derived neurons affected mitochondrial health and neuronal development (Gunnewiek et al., 2019; Motori et al., 2020), including upregulation of genes involved in cholesterol homeostasis (*INSIG1* and *LDLR*; Jensen et al., 2019). Although the ethanol concentration used varied (17 mM in our study vs 50 mM in Jensen et al., 2019), the results are similar. The top 2 upregulated genes in our 7 d ethanol exposure paradigm (*ANGPTL4* and *PDK4*; Fig. 3*B*) are also key players in lipid metabolism; *PDK4* in particular has been associated with a loss of metabolic flexibility (Zhang et al., 2014; Jeon et al., 2020) and disrupted mitochondrial homeostasis (Ma et al., 2019). Notably, GIRK channel activity is potentiated by cholesterol (Glaaser and Slesinger, 2017; Mathiharan et al., 2020), suggesting that changes in membrane cholesterol could impact GIRK function.

In parallel with maintaining intracellular calcium dynamics, ↑GIRK2 neurons appeared to preserve normal mitochondrial function, regardless of ethanol exposure (7- and 21 d IEE) or activity-dependent energy demands. In contrast, stimulation of neuronal activity in iso-CTL neurons with glutamate revealed an impairment in ATP-linked respiration after 7 d IEE, indicating a difficulty in meeting activity-dependent energy demands. Furthermore, after 21 d IEE, glutamate eliminated the increase of ATP-linked respiration in iso-CTL neurons. The reduction of ATP-linked respiration with the application of glutamate may be attributable to increased calcium influx and the disruption of mitochondrial membrane potential (Giorgi et al., 2018; Verma et al., 2022). SynGO analysis of combined ↑GIRK2 and IEE points to regulation of synaptic translation as a potential mechanism underlying the apparent preservation of normal mitochondrial function.

Previous studies investigating the role of GIRK2 expression in neuronal health showed somewhat conflicting outcomes. One study demonstrated that GIRK2 expression in TH-positive substantia nigra dopaminergic neurons is a vulnerability factor to mitochondrial stress and apoptosis (Chung et al., 2005). Another found that GIRK2 is upregulated in response to neurotoxins such as $A\beta_{42}$ in hippocampal dissociated cultures, potentially triggering $p75^{NTR}$ mediated cell death (May et al., 2017). Notably, $A\beta_{42}$ has an excitotoxic effect similar to the consequences of long-term ethanol exposure (Esposito et al., 2013), and therefore GIRK2 upregulation could be a protective measure. Further studies, including mitochondrial imaging and viability assays, are required to shed light on mechanisms underlying the relationship between GIRK2 expression, presynaptic calcium-dependent regulation of neurotransmitter release, synaptic translation, and mitochondrial function.

Future perspectives

In the current study, we focused on glutamatergic neurons due to their primary role in addiction (Burnett et al., 2016). Given the broad expression of GIRK channels as well as the regional and cell-type variability of their impact on neuronal activity, however, our observation could be unique to maturing glutamatergic neurons in the absence of inhibitory control. Future work should investigate mono- and cocultures with GABAergic and dopaminergic neurons, given the role of GIRK channels in facilitating $GABA_B$ and D_2 receptor function (Lüscher and Slesinger, 2010). Furthermore, 3D models such as assembloids and organoids can shed light on the role of GIRK2 and ethanol exposure on circuit development and neurodegenerative processes (Birey et al., 2017; Arzua et al., 2020; Szebényi et al., 2021). Differences in open state probability between GIRK2 homotetramer and GIRK1/2 heterotetramer channels (Rubinstein et al., 2009) also could play a role in neuronal excitability. Together, these future directions pave a path toward a cell- and circuit-level understanding of GIRK2-containing channels in human neurons and their influence on developmental and apoptotic processes affected by ethanol exposure.

Conclusions

In summary, we demonstrate that GIRK2 expression impacts the long-term effects of ethanol on neuronal activity and bioenergetics of glutamate neurons, suggesting a possible role for GIRK2 in mitigating dysfunctions caused by chronic alcohol use. Further investigations are necessary to determine the mechanisms underlying the intersection of GIRK channels, metabolism, and neuronal excitability and how they may vary in different neuronal cell types. Several key questions remain, including whether basal GIRK channel activity is essential for preserving mitochondrial function and whether increasing GIRK2 expression after the start of ethanol exposure would have a similar ameliorating effect. The relationship between GIRK2 activity and cellular respiration represents a potential new link with alcohol, opening a novel line of inquiry into the channel's role in neuronal health and resilience in the context of AUD. Initial levels of GIRK2 play a role in neuronal adaptations to ethanol and could therefore serve as predictors of pharmacotherapy response, allowing for the development of personalized treatments for AUD and prenatal alcohol exposure.

References

Aryal P, Dvir H, Choe S, Slesinger PA (2009) A discrete alcohol pocket involved in GIRK channel activation. Nat Neurosci 12:988–995.

Arzua T, Yan Y, Jiang C, Logan S, Allison RL, Wells C, Kumar SN, Schäfer R, Bai X (2020) Modeling alcohol-induced neurotoxicity using human induced pluripotent stem cell-derived three-dimensional cerebral organoids. Transl Psychiatry 10:347.

Bähring R, Barghaan J, Westermeier R, Wollberg J (2012) Voltage sensor inactivation in potassium channels. Front Pharmacol 3:100.

Bates D, et al. (2022) lme4: linear mixed-effects models using "Eigen" and S4. Available at: https://CRAN.R-project.org/package=lme4 [Accessed February 13, 2023].

Birey F, et al. (2017) Assembly of functionally integrated human forebrain spheroids. Nature 545:54–59.

Blednov YA, Stoffel M, Chang SR, Harris RA (2001a) GIRK2 deficient mice: evidence for hyperactivity and reduced anxiety. Physiol Behav 74:109–117.

Blednov YA, Stoffel M, Chang SR, Harris RA (2001b) Potassium channels as targets for ethanol: studies of G-protein-coupled inwardly rectifying potassium channel 2 (GIRK2) null mutant mice. J Pharmacol Exp Ther 298:521–530.

Bodhinathan K, Slesinger PA (2014) Alcohol modulation of G-protein-gated inwardly rectifying potassium channels: from binding to therapeutics. Front Physiol 5:76.

Borchers HW (2022) Pracma: practical numerical math functions. Available at: https://CRAN.R-project.org/package=pracma [Accessed February 13, 2023].

Burnett EJ, Chandler LJ, Trantham-Davidson H (2016) Glutamatergic plasticity and alcohol dependence-induced alterations in reward, affect and cognition. Prog Neuropsychopharmacol Biol Psychiatry 65:309–320.

Cassano T, Pace L, Bedse G, Lavecchia AM, De Marco F, Gaetani S, Serviddio G (2016) Glutamate and mitochondria: two prominent players in the oxidative stress-induced neurodegeneration. Curr Alzheimer Res 13:185–197.

Chorlian DB, et al. (2017) Genetic correlates of the development of theta event related oscillations in adolescents and young adults. Int J Psychophysiol 115:24–39.

Chung HJ, Ge W-P, Qian X, Wiser O, Jan YN, Jan LY (2009) G protein-activated inwardly rectifying potassium channels mediate depotentiation of long-term potentiation. Proc Natl Acad Sci U S A 106: 635–640.

Chung CY, Seo H, Sonntag KC, Brooks A, Lin L, Isacson O (2005) Cell type-specific gene expression of midbrain dopaminergic neurons reveals molecules involved in their vulnerability and protection. Hum Mol Genet 14: 1709–1725.

Cippitelli A, et al. (2017) Protection against alcohol-induced neuronal and cognitive damage by the PPARγ receptor agonist pioglitazone. Brain Behav Immun 64:320–329.

Das SC, Althobaiti YS, Alshehri FS, Sari Y (2016) Binge ethanol withdrawal: effects on post-withdrawal ethanol intake, glutamate-glutamine cycle and monoamine tissue content in P rat model. Behav Brain Res 303:120–125.

Desch K, Langer JD, Schuman EM (2021) Dynamic bi-directional phosphorylation events associated with the reciprocal regulation of synapses during homeostatic up- and down-scaling. Cell Rep 36:109583.

Duménieu M, Oulé M, Kreutz MR, Lopez-Rojas J (2017) The segregated expression of voltage-gated potassium and sodium channels in neuronal membranes: functional implications and regulatory mechanisms. Front Cell Neurosci 11:115.

Esposito Z, Belli L, Toniolo S, Sancesario G, Bianconi C, Martorana A (2013) Amyloid β, glutamate, excitotoxicity in Alzheimer's disease: are we on the right track? CNS Neurosci Ther 19:549–555.

Federici M, Nisticò R, Giustizieri M, Bernardi G, Mercuri NB (2009) Ethanol enhances GABAB-mediated inhibitory postsynaptic transmission on rat midbrain dopaminergic neurons by facilitating GIRK currents. Eur J Neurosci 29:1369–1377.

Fourcaud-Trocmé N, Zbili M, Duchamp-Viret P, Kuczewski N (2022) Afterhyperpolarization promotes the firing of mitral cells through a voltage-dependent modification of action potential threshold. eNeuro 9: ENEURO.0401-21.2021.

Germain P-L, Testa G (2017) Taming human genetic variability: transcriptomic meta-analysis guides the experimental design and interpretation of iPSC-based disease modeling. Stem Cell Rep 8:1784–1796.

Giorgi C, Marchi S, Pinton P (2018) The machineries, regulation and cellular functions of mitochondrial calcium. Nat Rev Mol Cell Biol 19:713–730.

Glaaser IW, Slesinger PA (2015) Structural insights into GIRK channel function. Int Rev Neurobiol 123:117–160.

Glaaser IW, Slesinger PA (2017) Dual activation of neuronal G protein-gated inwardly rectifying potassium (GIRK) channels by cholesterol and alcohol. Sci Rep 7:4592.

Gunnewiek TMK, et al. (2019) Mitochondrial dysfunction impairs human neuronal development and reduces neuronal network activity and synchronicity. bioRxiv:720227.

Halikere A, Popova D, Scarnati MS, Hamod A, Swerdel MR, Moore JC, Tischfield JA, Hart RP, Pang ZP (2020) Addiction associated N40D mu-opioid receptor variant modulates synaptic function in human neurons. Mol Psychiatry 25:1406–1419.

Hill KG, Alva H, Blednov YA, Cunningham CL (2003) Reduced ethanol-induced conditioned taste aversion and conditioned place preference in GIRK2 null mutant mice. Psychopharmacology 169:108–114.

Ho S-M, et al. (2017) Evaluating synthetic activation and repression of neuropsychiatric-related genes in hiPSC-derived NPCs, neurons, and astrocytes. Stem Cell Rep 9:615–628.

Ho S-M, Hartley BJ, Tcw J, Beaumont M, Stafford K, Slesinger PA, Brennand KJ (2016) Rapid Ngn2-induction of excitatory neurons from hiPSC-derived neural progenitor cells. Methods 101:113–124.

Jensen KP, Lieberman R, Kranzler HR, Gelernter J, Clinton K, Covault J (2019) Alcohol-responsive genes identified in human iPSC-derived neural cultures. Transl Psychiatry 9:96.

Jeon J-H, Thoudam T, Choi EJ, Kim M-J, Harris RA, Lee I-K (2020) Loss of metabolic flexibility as a result of overexpression of pyruvate dehydrogenase kinases in muscle, liver and the immune system: therapeutic targets in metabolic diseases. J Diabetes Investig 12:21.

Johnson MA, Weick JP, Pearce RA, Zhang S-C (2007) Functional neural development from human embryonic stem cells: accelerated synaptic activity via astrocyte coculture. J Neurosci 27:3069–3077.

Jones KA, Porjesz B, Chorlian D, Rangaswamy M, Kamarajan C, Padmanabhapillai A, Stimus A, Begleiter H (2006) S-transform time-frequency analysis of P300 reveals deficits in individuals diagnosed with alcoholism. Clin Neurophysiol 117:2128–2143.

Kamarajan C, et al. (2017) A KCNJ6 gene polymorphism modulates theta oscillations during reward processing. Int J Psychophysiol 115:13–23.

Kang SJ, et al. (2012) Family-based genome-wide association study of frontal theta oscillations identifies potassium channel gene KCNJ6. Genes Brain Behav 11:712–719.

Kim KC, Go HS, Bak HR, Choi CS, Choi I, Kim P, Han S-H, Han SM, Shin CY, Ko KH (2010) Prenatal exposure of ethanol induces increased glutamatergic neuronal differentiation of neural progenitor cells. J Biomed Sci 17:85.

Koopmans F, et al. (2019) SynGO: an evidence-based, expert-curated knowledge base for the synapse. Neuron 103:217–234.e4.

Kuzhikandathil EV, Oxford GS (2002) Classic D1 dopamine receptor antagonist R-(+)-7-chloro-8-hydroxy-3-methyl-1-phenyl-2,3,4,5-tetrahydro-1H-3-benzazepine hydrochloride (SCH23390) directly inhibits G protein-coupled inwardly rectifying potassium channels. Mol Pharmacol 62: 119–126.

Läck AK, Diaz MR, Chappell A, DuBois DW, McCool BA (2007) Chronic ethanol and withdrawal differentially modulate pre- and postsynaptic function at glutamatergic synapses in rat basolateral amygdala. J Neurophysiol 98:3185–3196.

La Paglia L, Listì A, Caruso S, Amodeo V, Passiglia F, Bazan V, Fanale D (2017) Potential role of ANGPTL4 in the cross talk between metabolism and cancer through PPAR signaling pathway. PPAR Res 2017:e8187235.

León BE, Kang S, Franca-Solomon G, Shang P, Choi D-S (2022) Alcohol-induced neuroinflammatory response and mitochondrial dysfunction on aging and Alzheimer's disease. Front Behav Neurosci 15: 778456.

Lieberman R, Levine ES, Kranzler HR, Abreu C, Covault J (2012) Pilot study of iPS-derived neural cells to examine biological effects of alcohol on human neurons in vitro. Alcohol Clin Exp Res 36:1678–1687.

Ligges U, et al. (2021) Signal: signal processing. Available at: https://CRAN.R-project.org/package=signal [Accessed February 13, 2023].

Lim JR, Chae CW, Park JY, Jung YH, Yoon JH, Kim MJ, Lee HJ, Choi GE, Han HJ (2023) Ethanol-induced ceramide production causes neuronal apoptosis by increasing MCL-1S-mediated ER-mitochondria contacts. Neurobiol Dis 177:106009.

Long JA (2022) Jtools: analysis and presentation of social scientific data. Available at: https://CRAN.R-project.org/package=jtools [Accessed February 13, 2023].

Loya A, Pnueli L, Yosefzon Y, Wexler Y, Ziv-Ukelson M, Arava Y (2008) The 3′-UTR mediates the cellular localization of an mRNA encoding a short plasma membrane protein. RNA 14:1352–1365.

Lüscher C, Slesinger PA (2010) Emerging concepts for G protein-gated inwardly rectifying potassium (GIRK) channels in health and disease. Nat Rev Neurosci 11:301–315.

Ma W-Q, Sun X-J, Wang Y, Zhu Y, Han X-Q, Liu N-F (2019) Restoring mitochondrial biogenesis with metformin attenuates β-GP-induced phenotypic transformation of VSMCs into an osteogenic phenotype via inhibition of PDK4/oxidative stress-mediated apoptosis. Mol Cell Endocrinol 479:39–53.

Mathiharan YK, Glaaser IW, Zhao Y, Robertson MJ, Skiniotis G, Slesinger PA (2020) Structural basis of GIRK2 channel modulation by cholesterol and PIP2. bioRxiv:2020.06.04.134544.

May LM, Anggono V, Gooch HM, Jang SE, Matusica D, Kerbler GM, Meunier FA, Sah P, Coulson EJ (2017) G-Protein-coupled inwardly rectifying potassium (GIRK) channel activation by the p75 neurotrophin receptor is required for amyloid β toxicity. Front Neurosci 11:455.

Mayfield J, Blednov YA, Harris RA (2015) Behavioral and genetic evidence for GIRK channels in the CNS: role in physiology, pathophysiology, and drug addiction. Int Rev Neurobiol 123:279–313.

Motori E, Atanassov I, Kochan SMV, Folz-Donahue K, Sakthivelu V, Giavalisco P, Toni N, Puyal J, Larsson N-G (2020) Neuronal metabolic rewiring promotes resilience to neurodegeneration caused by mitochondrial dysfunction. Sci Adv 6:eaba8271.

Odawara A, Saitoh Y, Alhebshi AH, Gotoh M, Suzuki I (2014) Long-term electrophysiological activity and pharmacological response of a human induced pluripotent stem cell-derived neuron and astrocyte co-culture. Biochem Biophys Res Commun 443:1176–1181.

Popova D, et al. (2023) Alcohol reverses the effects of KCNJ6 (GIRK2) non-coding variants on excitability of human glutamatergic neurons. Mol Psychiatry 28:746–758.

R Core Team (2020) R: a language and environment for statistical computing. Available at:

Rangaswamy M, et al. (2007) Delta and theta oscillations as risk markers in adolescent offspring of alcoholics. Int J Psychophysiol 63:3–15.

Ransdell JL, Moreno JD, Bhagavan D, Silva JR, Nerbonne JM (2022) Intrinsic mechanisms in the gating of resurgent Na+ currents Giraldez T, Aldrich RW, Giraldez T, eds. Elife 11:e70173.

Rubinstein M, Peleg S, Berlin S, Brass D, Keren-Raifman T, Dessauer CW, Ivanina T, Dascal N (2009) Divergent regulation of GIRK1 and GIRK2 subunits of the neuronal G protein gated K+ channel by GαiGDP and Gβγ. J Physiol 587:3473–3491.

Savell KE, et al. (2018) A neuron-optimized CRISPR/dCas9 activation system for robust and specific gene regulation. bioRxiv:371500.

Scarnati MS, Boreland AJ, Joel M, Hart RP, Pang ZP (2020) Differential sensitivity of human neurons carrying μ opioid receptor (MOR) N40D variants in response to ethanol. Alcohol 87:97–109.

Schindelin J, et al. (2012) Fiji: an open-source platform for biological-image analysis. Nat Methods 9:676–682.

Schreibmayer W, Dessauer CW, Vorobiov D, Gilman AG, Lester HA, Davidson N, Dascal N (1996) Inhibition of an inwardly rectifying K + channel by G-protein α-subunits. Nature 380:624.

Slesinger PA, Stoffel M, Jan YN, Jan LY (1997) Defective gamma-aminobutyric acid type B receptor-activated inwardly rectifying K+ currents in cerebellar granule cells isolated from weaver and Girk2 null mutant mice. Proc Natl Acad Sci U S A 94:12210–12217.

Soni A, Klütsch D, Hu X, Houtman J, Rund N, McCloskey A, Mertens J, Schafer ST, Amin H, Toda T (2021) Improved method for efficient generation of functional neurons from murine neural progenitor cells. Cells 10:1894.

Sun J, Wu D, Wong GC-N, Lau M, Yang M, Hart RP, Kwan K-M, Chan E, Chow H-M (2023) Chronic alcohol metabolism results in DNA repair infidelity and cell cycle-induced senescence in neurons. Aging Cell 22:e13772.

Szebényi K, et al. (2021) Human ALS/FTD brain organoid slice cultures display distinct early astrocyte and targetable neuronal pathology. Nat Neurosci 24:1542–1554.

Tang X, Zhou L, Wagner AM, Marchetto MCN, Muotri AR, Gage FH, Chen G (2013) Astroglial cells regulate the developmental timeline of human neurons differentiated from induced pluripotent stem cells. Stem Cell Res 11:743–757.

Tapia-Rojas C, Pérez MJ, Jara C, Vergara EH, Quintanilla RA (2017) *Mitochondrial Dis*.

Tarazona S, Furió-Tarí P, Turrà D, Pietro AD, Nueda MJ, Ferrer A, Conesa A (2015) Data quality aware analysis of differential expression in RNA-seq with NOISeq R/Bioc package. Nucleic Acids Res 43:e140.

Tcw J, et al. (2017) Divergent levels of marker chromosomes in an hiPSC-based model of psychosis. Stem Cell Rep 8:519–528.

Tiscornia G, Singer O, Verma IM (2006) Production and purification of lentiviral vectors. Nat Protocols 1:241–245.

Topol A, et al. (2016) Dysregulation of miRNA-9 in a subset of schizophrenia patient-derived neural progenitor cells. Cell Rep 15: 1024–1036.

Vandecasteele G, Szabadkai G, Rizzuto R (2001) Mitochondrial calcium homeostasis: mechanisms and molecules. IUBMB Life 52:213–219.

Verma M, Lizama BN, Chu CT (2022) Excitotoxicity, calcium and mitochondria: a triad in synaptic neurodegeneration. Transl Neurodegener 11:3.

Victoria NC, de Velasco EMF, Ostrovskaya O, Metzger S, Xia Z, Kotecki L, Benneyworth MA, Zink AN, Martemyanov KA, Wickman K (2016) G protein-gated K+ channel ablation in forebrain pyramidal neurons selectively impairs fear learning. Biol Psychiatry 80:796–806.

Walter NAR, Denmark DL, Kozell LB, Buck KJ (2017) A systems approach implicates a brain mitochondrial oxidative homeostasis co-expression network in genetic vulnerability to alcohol withdrawal. Front Genet 7:218.

Warner H, Mahajan S, van den Bogaart G (2022) Rerouting trafficking circuits through posttranslational SNARE modifications. J Cell Sci 135: jcs260112.

Wickham H, Chang W, Henry L, Pedersen TL, Takahashi K, Wilke C, Woo K, Yutani H, Dunnington D, RStudio (2023) Ggplot2: create elegant data visualisations using the grammar of graphics. Available at: https://CRAN.R-project.org/package=ggplot2 [Accessed February 13, 2023].

Yang N, et al. (2017) Generation of pure GABAergic neurons by transcription factor programming. Nat Methods 14:621.

Yu Z, Guindani M, Grieco SF, Chen L, Holmes TC, Xu X (2022) Beyond t test and ANOVA: applications of mixed-effects models for more rigorous statistical analysis in neuroscience research. Neuron 110:21–35.

Zhang Z-M, Chen S, Liang Y-Z (2010) Baseline correction using adaptive iteratively reweighted penalized least squares. Analyst 135:1138–1146.

Zhang S, Hulver MW, McMillan RP, Cline MA, Gilbert ER (2014) The pivotal role of pyruvate dehydrogenase kinases in metabolic flexibility. Nutr Metab 11:10.

Zhao Y, et al. (2020) Identification of a G-protein-independent activator of GIRK channels. Cell Rep 31:107770.